

Metabolic plasticity of HIV-specific CD8+ T cells is associated with enhanced antiviral potential and natural control of HIV-1 infection

Mathieu Angin, Stevenn Volant, Caroline Passaes, Camille Lecuroux, Valerie Monceaux, Marie-Agnès Dillies, Jose Carlos Valle-Casuso, Gianfranco Pancino, Bruno Vaslin, Roger Le Grand, et al.

▶ **To cite this version:**

Mathieu Angin, Stevenn Volant, Caroline Passaes, Camille Lecuroux, Valerie Monceaux, et al.. Metabolic plasticity of HIV-specific CD8+ T cells is associated with enhanced antiviral potential and natural control of HIV-1 infection. Nature Metabolism, 2019, 1, pp.704-716. 10.1038/s42255-019-0081-4 . pasteur-02549933

HAL Id: pasteur-02549933
https://pasteur.hal.science/pasteur-02549933

Submitted on 21 Apr 2020

HAL is a multi-disciplinary open access archive for the deposit and dissemination of scientific research documents, whether they are published or not. The documents may come from teaching and research institutions in France or abroad, or from public or private research centers.

L'archive ouverte pluridisciplinaire **HAL**, est destinée au dépôt et à la diffusion de documents scientifiques de niveau recherche, publiés ou non, émanant des établissements d'enseignement et de recherche français ou étrangers, des laboratoires publics ou privés.



Distributed under a Creative Commons Attribution - NonCommercial 4.0 International License

Metabolic plasticity of HIV-specific CD8+ T-cells is associated with enhanced antiviral potential and natural control of HIV-1 infection.

Mathieu Angin[1], Stevenn Volant[2], Caroline Passaes[1], Camille Lecuroux[3], Valérie Monceaux[1], Marie-Agnes Dillies[2], José Carlos Valle Casuso[1], Gianfranco Pancino[1], Bruno Vaslin[3], Roger Le Grand[3], Laurence Weiss[4,5], Cecile Goujard[6], Laurence Meyer[7], Faroudy Boufassa[7], Michaela Müller-Trutwin[1], Olivier Lambotte[3,6], and Asier Sáez-Cirión[1]

[1]Institut Pasteur, Unité HIV Inflammation et Persistance, Paris, France

[2]Institut Pasteur, Hub Bioinformatique et Biostatistique – C3BI, USR 3756 IP CNRS – Paris, France

[3]CEA, Université Paris Sud, INSERM U1184, Immunology of Viral Infections and Autoimmune Diseases (IMVA), IDMIT Department / IBFJ, 92265 Fontenay-aux-Roses, France

[4]Assistance Publique Hôpitaux de Paris, Hôpital Européen Georges Pompidou, Paris, France

[5]Université Paris Descartes, Sorbonne Paris Cité, Paris, France

[6]Assistance Publique Hôpitaux de Paris, Hôpital Bicêtre, Service de Médecine Interne et Immunologie clinique, 94275 Le Kremlin-Bicêtre, France

[7]INSERM U1018, Centre de recherche en Epidémiologie et Santé des Populations, Université Paris Sud, Le Kremlin Bicêtre, France

Corresponding author:

Asier Sáez-Cirión: Unité HIV Inflammation et Persistance, Institut Pasteur, 28 rue du Docteur Roux, 75724 Paris Cedex 15, France. Tel.: 33-145-688-768. Fax: 33-145-688-957.

E-mail: asier.saez-cirion@pasteur.fr

ABSTRACT

Spontaneous control of HIV is generally associated with an enhanced capacity of CD8+ T-cells to eliminate infected CD4+ T-cells, but the molecular characteristics of these highly functional CD8+ T-cells are largely unknown. Here, using single-cell analysis, we show that HIV-specific central memory CD8+ T-cells from spontaneous HIV controllers (HIC) and antiretroviral-treated non-controllers have opposing transcriptomic profiles. Genes linked to effector functions and survival are upregulated in cells from HIC. In contrast, genes associated with activation, exhaustion and glycolysis are upregulated in cells from non-controllers. We show that HIV-specific CD8+ T-cells from non-controllers are largely glucose-dependent, while those from HIC have more diverse metabolic resources that enhance both their survival potential and their capacity to develop anti-HIV effector functions. The functional efficiency of the HIV-specific CD8+ T-cell response in HIC is thus engraved in their memory population and related to their metabolic program. Metabolic reprogramming in vitro through IL-15 treatment abrogated the glucose dependency and enhanced the antiviral potency of HIV-specific CD8+ T-cells from non-controllers.

INTRODUCTION

HIV-1-specific CD8+ T-cells develop promptly following HIV-1 infection and contribute to limiting viremia. However, they do not fully control the virus and their functions weaken further during chronic infection[1]. When compared to CD8+ T-cells elicited by other pathogens, HIV-specific CD8+ T-cells show delayed maturation and limited effector potential[2,3]. However, HIV-specific CD8+ T-cells endued with enhanced proliferative capacity[4], polyfunctionality[5] and cytotoxicity[6] have been described in rare individuals (HIV controllers, HIC) who maintain the virus below the detection limit without antiretroviral therapy[7]. HLA B*27 and B*57 are over-represented among HIC, further supporting a role of CD8+ T-cells in HIV control. Natural control of HIV infection is also usually associated with an ability of HIV-specific CD8+ T-cells to efficiently eliminate HIV-infected autologous CD4+ T-cells *ex vivo*[8]. Similar activity can also be found in HIV-2-controllers[9], but not during the acute or chronic stage of HIV-1 infection in individuals who do not control infection[10,11]. Superior virus-inhibiting activity has been attributed to all memory CD8+ T-cell subsets from HIC[12], pointing to intrinsic differences between cells from controllers and non-controllers.

Here we aimed to identify inherent differences between HIV-specific CD8 from HIC and those from HIV non-controllers with suppressed viremia on antiretroviral treatment (cART). We focused the analysis on central memory CD8+ T (CD8+ TCM)-cells, which represent an intermediate state between naïve and effector CD8+ T-cells and are responsible for long-term immune memory responses[13]. We postulated that any intrinsic differences between cells from HIC and non-controllers should be already imprinted in the CD8+ TCM subset. HIV-infected individuals with low virus set-points have significantly larger numbers of CD8+ TCM[14], while HIV disease progression is associated with shorter CD8+ TCM lifespans and numbers[15], highlighting their role in HIV control. However, CD8+ TCM cells are heterogeneous and have variable potential for proliferation and differentiation[16].

We conducted single-cell gene expression analyses, as this approach is well-adapted to identify differences between cells that have the same phenotype in methods such as conventional flow cytometry[17]. We found that HIV-specific CD8+ TCM cells from HIC and non-controllers had distinct transcriptional signatures. Our findings reveal that metabolic plasticity is an important characteristic of efficient HIV-specific CD8+ T-cells that better equipped them to survive and to counteract the virus. We demonstrate that metabolic reprogramming in vitro of HIV-specific CD8+ T-cells from non-controllers enhanced their antiviral potency.

RESULTS

Strong anti-HIV potential of HIC central memory CD8+ T-cells

CD8+ T-cells with a strong capacity to suppress HIV infection of autologous CD4+ T-cells *ex vivo* can be isolated from HIC but not from cART individuals[8,10,18] (Figure 1A). Here, we first investigated whether this capacity of HIC CD8+ T-cells could be found among naïve, central memory, transitional memory and effector memory CD8+ T-cell subsets (Supplementary Figure 1). As expected, naïve CD8+ T-cells from HIC had no HIV-suppressive capacity. In contrast, all sorted memory CD8+ T-cell subsets from HIC, but not from cART individuals, suppressed HIV infection as efficiently as bulk CD8+ T-cells (Figure 1B). Therefore, although effector memory cells likely had more immediate anti-viral capacity[12], HIV-specific CD8+ TCM-cells from HIC can efficiently react to counteract HIV-1 infection during the co-culture. These results support the view that the strong antiviral potential of HIC is already embedded in the program of their HIV-specific CD8+ TCM-cells.

Distinct gene expression profile in HIV-specific CD8+ TCM-cells from HIC

We then compared the single-cell gene expression profiles (96 genes associated with CD8+ T-cell function, differentiation, metabolism and survival (Supplementary Figure 2, Supplementary Data 1)) of HIV-specific CD8+ TCM cells from five HIC whose CD8+ T-cells had strong HIV-suppressive capacity and from five cART individuals (Supplementary Table 1). Cells from cART and HIC analyzed here shared not only the same differentiation status but also the same activation phenotype, as defined by flow cytometry (Figure 1C, Supplementary Table 2). Despite their similar phenotype, t-sne (t-distributed stochastic neighbor embedding algorithm) based analysis showed that HIC and cART cells had distinct gene expression profiles (Figure 1D), with stronger group differences between cells from HIC and cART than differences among cells from individuals in each group ($p=0.003$ for inter-group vs intra-group variance).

Upregulation of antiviral genes in HIV-specific CD8+ TCM-cells from HIC

Next, we analyzed the genes differently expressed in HIV-specific CD8+ TCM-cells from HIC and cART individuals. At the single-cell level, gene expression is not continuous but occurs in pulses, with periods of inactivity[7]. We therefore analyzed our data using MAST (Model-based Analysis of Single Cell Transcriptomics), which identified differently expressed genes (i) considering only the expressed genes (continuous, e.g. differences in mRNA expression levels); (ii) considering expressed vs non-expressed genes (discrete, i.e. differences in the frequency of cell expressing or not that gene); (iii) combining the discrete and continuous parts of the model (hurdle).

Overall, differences between cells from HIC and cART individuals were found for 38 genes (23 genes in the continuous analysis, 21 in the discrete analyses; 33 genes were found in the hurdle analysis; Supplementary Figures 3 and 4, Supplementary table 3). Ten genes relating to CD8+ T-cell effector activities were found to be more frequently active and/or expressed at higher levels in HIV-specific CD8+ TCM-cells from HIC than in those from cART (Figure 2). These genes included beta-chemokines (*CCL3*, *CCL3L1* and *XCL1)*, which interfere with HIV-1 infection[19]; granzymes (*GZMB*, *GZMK*), which are major mediators of CD8+ T-cell antiviral cytotoxic activities[6]; and other molecules involved in CD8+ T-cell-induced apoptosis, such as Fas ligand (*FASL*), tumor necrosis factor (*TNF*) and TNF-related apoptosis-inducing ligand (*TRAIL/TNFSF10*). Intriguingly, although CD8+ T-cells are not considered to be major producers of type-I interferon, we found that cells from HIC expressed *IFNB* transcripts at higher levels than cells from cART. Only *PRF1* showed higher expression in cells from cART individuals. These results show that HIV-specific CD8+ TCM-cells are endowed with massive antiviral potential, in keeping with our demonstration that CD8+ TCM-cells from HIC efficiently suppress HIV infection *ex vivo*.

Upregulation of cell survival genes in HIV-specific CD8+ TCM-cells from HIC

We then analyzed the nature of the other 28 genes differently expressed in cells from HIC and cART (see Supplementary figure 5 for not differently expressed genes). Cells from cART more frequently expressed genes linked to activation (*CD69, KLRD1*) than cells from HIC (Figure 3A), despite similar surface expression of HLA-DR and CD38 (Figure 1C, Supplementary Table 2). Cells from cART also expressed *CD8A* mRNA and the inhibitory regulators *LAG-3* and *CDKN1B*, more frequently and/or at higher levels (Figure 3A), in line with their more highly activated profile. Cells from cART also more frequently expressed interferon-stimulated genes (*MX1, OAS1*) and *HIF1A*, a gene linked to the mTOR pathway and glycolysis[20] (Figure 3A). Overall, the profile of cells from cART individuals was compatible with activation of mTORC1[20,21], which regulates cellular metabolism, and particularly anaerobic glycolysis, to keep up with energy requirements upon activation[22].

In contrast, cells from HIC expressed more frequently or at higher levels several key genes of the mTORC2 pathway (*RICTOR*, *CDC42, RHOA*) (Figure 3B), which has been linked to cell survival[23]. Indeed, cells from HIC also upregulated genes directly associated with cell survival and resistance to apoptosis (*IL7R*, *BCL2*, *EOMES*, *ID2*) (Figure 3B). Interestingly, HIC cells expressed higher levels of *VHL* (Figure 3B), which targets HIF-1 for proteasomal degradation[24] and counteracts HIF-1-mediated upregulation of glycolysis in CD8+ T-cells[25]. Thus, HIV-specific CD8+ TCM-cells from HIC not only expressed lower levels of *HIF1A* when compared to cART cells, but were also set to actively counter this factor. Cells from HIC also expressed higher levels of *REPIN1*, which is involved in metabolic regulation and downregulation of glucose transport[26]. Overall, these results suggest that HIV-specific CD8 TCM-cells from cART individuals are primed for activation and glycolysis, while cells from HIC are rather primed for survival through the mTORC2 pathway.

Effector function and survival genes are co-expressed in HIC cells

We explored whether differently expressed genes between HIV-specific CD8+ TCM-cells from HIC and cART individuals were inter-related, i.e. whether their respective expression profiles coincided in

individual cells. Although heterogeneity was observed, cells from HIC and cART segregated with opposing profiles (Figure 4): cells expressing the highest levels of effector function-related genes (e.g. *GZMB*, *CCL3*, *FASL*, *TNF, IFNB1*) also expressed high levels of genes associated with cell survival (*IL7R, BCL*-2, *ID2*) and were almost exclusively found in HIC. Moreover, these cells expressed relatively low levels of *CD8A*, *CD69*, *LAG3, KLRD1* and *HIF1A*, which were strongly expressed by cells from cART individuals (Figure 4A,B). These profiles support that HIC are characterized by the presence of HIV-specific CD8+ TCM-cells with high antiviral potential concomitantly primed for survival, while cART's cells have limited antiviral potential and exhibit upregulation of genes linked to glycolysis, senescence and exhaustion.

Shared gene expression profile in cells from HIC with strong and weak responses

Although most HIC have HIV-specific CD8+ T-cells that efficiently suppress the virus (strong responders, SR), some have weak CD8+ T-cell responses that fail to suppress HIV *ex vivo* (weak responders, WR)[18]. The differences between SR and WR cannot be explained by different HLA backgrounds, because the protective HLA B alleles are equally overrepresented in the two subgroups[27]. CD8+ T-cells from WR can recover their virus-suppressing capacity upon stimulated expansion[28]. We thus wondered whether HIV-specific CD8+ TCM-cells from WR and SR have the same transcription profile. We studied HIV-specific CD8+ TCM-cells from five WR (Supplementary Table 1) and found that their gene expression profile was intermediate between the SR and cART cells analyzed before (Figure 5A, Supplementary Table 4), although closer to that of SR. In particular, HIV-specific CD8+ TCM-cells from both WR and SR expressed higher levels of genes related to effector function (*CCL3L1*, *GZMB*, *IFNB, TNF*) (Figure 5B) (although less broadly for WR (Supplementary Figure 6)), and survival (*IL7R*, *PRKCA, ID2*) (Figure 5C) compared to cells from cART. As previously observed, cells from cART showed upregulation of genes linked to mTORC1/activation/glycolysis (*CD8A*, *HIF1A*, *KLRD1*, *CD69, IRF1*) and *LAG3* inhibitory receptor (Figure

178 5D) than both SR and WR. These data imply that HIV-specific CD8+ TCM-cells from HIC SR and WR
179 share a close transcriptome program despite their different functional activities *ex vivo*.
180
181 **Different metabolite uptake by CD8+ TCM cells from HIC and non-controllers**
182 We then explored if the changes in the transcriptional program of HIV-specific CD8+ TCM cells from
183 HIC and cART individuals translated in differences at the protein and functional level. We observed
184 that, although not statistically significant, HIC tended to carry more frequently cells with high levels
185 of GRZB than cART individuals (Figure 6A). HIF1 was more strongly expressed in HIV-specific CD8+
186 TCM-cells from cART individuals than in cells from HIC (figure 6A), strengthening our observations
187 that mTORC1 and glycolysis were particularly upregulated in the cells from non-controllers[20]. As
188 discussed above, cells from HIC showed upregulation of *VHL and REPIN1* (Figures 3B, 4) which may
189 downplay glycolysis by counteracting HIF1A and decreasing glucose transport[24,26]. This implies
190 different regulation of CD8+ T-cell metabolism in the two groups of individuals. The metabolic
191 activity of cells is tightly linked to their function. Activated effector cells preferentially upregulate
192 glycolysis to meet the energy demands imposed by T-cell proliferation, while memory cells rely on
193 fatty acid oxidation to fuel mitochondrial oxidative phosphorylation and persist[29]. CD8+ TCM-cells
194 from HIC exhibited ex vivo significantly higher fatty acid uptake than those from cART, whereas there
195 was no significant difference in glucose uptake (Figure 6B). In consequence, CD8+ TCM-cells from HIC
196 had a higher fatty acid/glucose uptake ratio than cells from cART individuals (Figure 6B).
197
198 **Glucose dependency of HIV-specific CD8+ T-cells from non-controllers.**
199 The above results suggest that HIV-specific CD8+ T-cells from cART individuals might be more
200 glucose-dependent than cells from HIC. We tested the capacity of CD8+ T-cells from HIC and cART
201 (Supplementary Table 5) to react against a pool of HIV-1 Gag peptides in the presence and absence of
202 glucose. We found that both TNF-α secretion and the overall magnitude of the HIV-specific CD8+ T-
203 cell response (Figure 7A, 7C) from both the HIC and cART groups were significantly diminished in the

absence of glucose. However, the HIV-specific CD8+ T-cell response from cART was more strongly impacted and barely detectable or undetectable without glucose (Figure 7A, 7C). In contrast, CMV-specific CD8+ T-cell responses from cART were not significantly impacted by glucose deprivation (Supplementary Figure 8). The viability of CD8+ T-cells from HIC and cART individuals also decreased in the absence of glucose, but cells from cART individuals again tended to be more strongly affected (Supplementary Figure 9). These functional tests support our gene expression results demonstrating that HIV-specific CD8+ T-cells from cART individuals are dependent predominantly on glucose in contrast to HIC.

We wondered if the detected profiles on blood cells were representative of tissue cells. We therefore analyzed the impact of glucose deprivation on SIV-specific CD8+ T-cell responses from lymphoid tissues of macaques spontaneously controlling SIVmac251 infection (SIV controllers, SIC) or not controlling (viremic, VIR) (Supplementary Figure 10A). In line with what we described for HIV-infected individuals, blood and splenic CD8+ T-cells from SIC, but not from viremic animals, had a strong capacity *ex vivo* to suppress SIV infection of autologous CD4+ T-cells (Supplementary Figure 10B). The splenic SIV-specific CD8+ T-cell response from SIC was not significantly affected by the absence of glucose, while it strongly decreased in conditions of glucose deprivation for viremic animals (Supplementary Figure 10C). These results confirm that strong glucose dependency is an inherent characteristic of the less efficient CD8+ T-cells found in non-controller subjects.

Metabolic plasticity of HIV-specific CD8+ T-cells from HIC

Since HIV-specific CD8+ T-cells from HIC still responded despite glucose deprivation, our data suggest that they mobilize additional energetic resources. We also noted a trend toward larger mitochondrial mass in cells from cART individuals (Supplementary Figure 11), a feature that has been linked to mitochondrial dysfunction in senescent CD8+ T-cells[30] and exhausted HBV-specific CD8+ T-cells[31]. We wondered if cells from HIC and cART might differ with respect to their mitochondrial function. We

found that menadione, a drug that alters mitochondrial membrane polarization[32], significantly reduced TNF-α and IFN-γ secretion and diminished the overall response of CD8+ T-cells from HIC but not cART individuals (Figure 7A, C, Supplementary Figure 12). Altogether, cells from HIC, in contrast to cells from cART, appear to rely on mitochondrial function to fuel their anti-HIV CD8+ T-cell responses in addition to glycolysis.

We found that metabolic plasticity was important for sustaining qualitative differences between CD8+ T-cells from HIC and non controllers. The polyfunctionality of HIV-specific CD8+ T-cells from HIC was higher than that of cells from cART individuals in control conditions, in accordance with previous reports[5]. The percentage of highly polyfunctional cells in HIC (3 or 4 functions) was not significantly altered in the absence of glucose (Figure 7B, 7C), but decreased significantly in the presence of menadione (Figure 7B, 7C). No significant changes were observed in the polyfunctionality of HIV-specific CD8+ T-cells from cART individuals in the absence of glucose or the presence of menadione. Highly polyfunctional cells were only observed in two cART individuals at very low frequencies, and they were still detectable in the absence of glucose but could not be detected in the presence of menadione. Thus, the polyfunctionality of CD8+ T-cells appeared to depend on mitochondrial function rather than on glycolysis, which suggests that not all CD8+ T-cell functions are equally controlled by the same metabolic pathways.

To further explore this possibility, we analyzed phosphorylation of ribosomal S6 (pS6) and AKT (pAKT) proteins, as markers, respectively, of engagement of mTORC1 and mTORC2 pathways, in CD8+ T-cells from HIC producing IFNγ or TNFα upon stimulation with HIV-1 Gag peptides. Interestingly, while IFNγ+ HIV-specific CD8+ T-cells were characterized by high levels of pS6 and low levels of pAKT (Supplementary Figure 13), the cells producing TNFα showed both high levels of pAKT and pS6, although not necessarily simultaneously (Supplementary Figure 13). Therefore, our results indicate that while IFNγ production, one of the last function to be lost in exhausted HIV-specific CD8+ T-

cells[33], is regulated by mTORC1, polyfunctionality might depend on mTORC2. Moreover, mTORC1 did not appear critical for CD8+ T-cells from HIC during our HIV/SIV-suppression assay. Rapamycin treatment during the suppression assay decreased the infection levels of isolated CD4+ T-cells (Supplementary Figure 14A), further showing that metabolic activities (and the mTORC1 pathway in particular) are critical for the establishment of HIV/SIV infection in CD4+ T-cells[34,35]. However, rapamycin did not abolish the capacity of CD8+ T-cells from HIV or SIV controllers to suppress infection (Supplementary Figure 14A). We could analyze oxidative phosphorylation and glycolysis in purified CD8+ T-cells from a limited number of HIC (n=3) and cART individuals (n=2) after co-culture with non-infected or HIV pre-infected autologous CD4+ T-cells. No differences in cell metabolism were observed between the CD8+ T-cells from cART individuals whether they had been cultured with infected or non-infected cells. In contrast, CD8+ T-cells from HIC cultured in presence of infected CD4 T-cells showed enhanced metabolic activities, and in particular oxidative phosphorylation when compared to CD8+ T-cells that had been cultured in presence of non-infected cells (Supplementary Figure 14B), suggesting that CD8+ T-cells from HIC mobilized different metabolic resources in presence of HIV infected CD4+ T-cells.

Our results globally indicate that the functions more commonly associated with efficient HIV-specific CD8+ T-cell responses in controllers (polyfunctionality, viral suppression capacity) are sustained by the mTORC2 pathway and rely on both glucose and oxidative phosphorylation, while cells from cART rely mostly on glucose metabolism. They strongly suggest that metabolic plasticity is a critical characteristic of highly efficient CD8+ T-cells.

IL-15 reinvigorates HIV-specific CD8+ T-cells from non-controllers

IL-15 promotes fatty acid oxidation and mitochondrial biogenesis in CD8+ T-cells[29]. Accordingly, we found that IL-15 pre-treatment enhanced the rates of fatty acid uptake and the basal metabolic activities and maximal mitochondrial respiratory capacity of bulk CD8+ T-cells from cART individuals

(Figure 8A and B). IL-15 increased the frequency of HIV-specific CD8+ T-cell responses in cART but it did not alter the frequency of CMV-specific CD8+ T-cells in the same individuals (Figure 8C). Importantly, IL-15 pre-treatment also strongly enhanced the capacity of CD8+ T-cells from cART individuals to suppress HIV infection (Figure 8D). IL-15 pre-treatment was also able to increase the SIV-CD8+ T-cell response in lymphoid tissues of SIV viremic animals, abrogated their glucose dependency (Supplementary Figure 10C) and strongly increased their capacity to suppress SIV infection of CD4+ T-cells (Supplementary Figure 10D). These results show that metabolic reprogramming rescues HIV/SIV-specific CD8+ T-cell responses in non-controller individuals and further confirm that metabolic plasticity is a critical element in the efficacy of the HIV-specific CD8+ T-cell response.

293

294 **DISCUSSION**

295 Durable natural HIV control has been linked to the presence of HIV-specific CD8+ T-cells with
296 enhanced capacities in functional assays *in vitro*[8]. We show here that the superior antiviral potential
297 of CD8+ T-cells from HIC is engraved in the transcriptional program of the central memory
298 population. When compared to cells from non-controllers, CD8+ TCM-cells from HIC exhibited
299 upregulation of a broad range of genes linked to effector functions, indicating that differences
300 between HIC and cART HIV-specific CD8+ T-cell responses are related to different memory-cell
301 programs rather than to the accumulation of flaws in non-controllers' effector cells. Cells from HIC
302 upregulated genes linked to survival, while cells from non-controllers upregulated genes associated
303 with mTORC1 activation and glycolysis. Functional analyses showed that HIV-specific CD8+ T-cells
304 from HIC had metabolic plasticity while cells from non-controllers had a strong dependency on
305 glycolysis, and similar results were obtained in tissues from a non-human primate model of durable
306 SIVmac251 control. Pre-treatment with IL-15 reinvigorated HIV/SIV-specific CD8+ T-cell responses in
307 non-controllers, ablating their dependency on glucose and enhancing their capacity to suppress
308 infection.

309

310 Our results show that HIV-specific CD8+ T-cells from controllers are equipped with a large panel of
311 mechanisms to counteract HIV infection, including soluble antiviral factors and direct cytotoxic
312 activities. The different expression of T-cell "function" genes between HIC and cART was
313 accompanied by different expression of other sets of genes indicating the preferential activation of
314 mTORC1 in cART individuals and mTORC2 in HIC. mTORC1 and mTORC2 play distinct roles in CD8+ T-
315 cell differentiation. mTORC1 is generally associated with the induction of glycolysis and the
316 generation of effector cells, while mTORC2 is linked to the regulation of T-cell memory functions[22].
317 Expression of genes associated with mTORC1 in HIV-specific CD8+ TCM-cells from cART individuals
318 points to a skewed priming of these cells. On the other hand, strong expression of effector-linked

319 genes in cells from HIC was accompanied by very weak expression of mTORC1-linked genes. We
320 show here that production of IFN-γ and TNFα by HIV-specific CD8+ T-cells from HIC were associated
321 with different engagement of mTORC1 and mTORC2. Moreover, mTORC1 blocking with rapamycin
322 did not diminish the capacity of CD8+ T-cells from controllers to suppress infection. It is still unclear
323 which processes are controlled by mTORC1 during effector functioning and, although mTORC1
324 activation appears necessary for IFN-γ production, our results are in agreement with previous reports
325 indicating that this pathway may not have a global impact on cytokine production[36].
326
327 HIV-specific CD8+ TCM-cells from HIC also exhibited upregulation of genes linked to survival, while
328 cells from cART rather had a pro-apoptotic signature. Susceptibility of HIV-specific CD8+ T-cells to
329 apoptosis is well documented in non-controllers[2,37]. Effector memory CD8+ T-cells isolated from HIC
330 are preserved after prolonged culture, while HIV-specific CD8+ T-cells from non-controllers are
331 gradually lost in the same conditions[38]. Indeed, it is possible that the enhanced capacity of CD8+ T-
332 cells from HIC to suppress HIV infection results from the combination of higher cytotoxic potential on
333 a per-cell basis[6] and enhanced survival of the cells in absence of cytokines as required in the
334 suppression assay prior to the co-culture[8]. Overall, our results indicate that HIV-specific CD8+ T-cells
335 from HIC are better equipped to survive, including in conditions of metabolic stress, which may be an
336 indication of enhanced stemness of these cells[39].
337
338 Our results support the notion that differences in the functionality of HIV-specific CD8+ T-cells from
339 HIC and non-controllers are imprinted in the program of their memory cells. While exhaustion is
340 typically associated with effector T-cells having a very limited capacity to establish persistent
341 memory[40], HIV-specific CD8+ T-cells from the cART individuals studied here were characterized by a
342 profile reminiscent of exhausted cells, including the concomitant upregulation of genes encoding
343 several inhibitory receptors (e.g. *LAG3, KLRD1*), despite their central memory phenotype. This

supports the notion that exhausted CD8+ T-cells may represent a distinct subset of cells that have received specific differentiation priming[41].

HIV-specific CD8+ CM T-cells from HIC patients classified as strong or weak responders in terms of the direct antiviral activity of their CD8+ T-cells *ex vivo*[18] shared many features and similarly differ of cells from non-controllers. When compared to SR HIC, WR HIC generally had lower ultrasensitive viral load[27] and a lower frequency of infected cells with reactivable virus[42], and likely constitute a subgroup of HIC who have achieved tighter control of the infection. Accordingly, our results show that the responses of HIV-specific CD8+ T-cells from SR and WR receive similar priming, although the profile of cells from WR HIC reflects a longer period of quiescence[18].

One possible limitation to our single cell analyses is that, due to sample availability, not all sorted CM cells had the same HIV antigen specificity, which might have some impact on their molecular program. However single cells from HIC and ART individuals showed a compelling segregation. Moreover, the direct comparison of cells from subjects HIC 01001 and ART 630104, which were sorted with the same dextramer (A03 Gag 020-028), recapitulated many of the differences that were found in the global analysis (Supplementary Figure 15), confirming that main differences between cells from HIC and ART were not related to epitope specificity.

Our findings suggest that the survival and functional advantages of HIV-specific CD8+ T-cells from HIC might be related to their greater metabolic plasticity. Indeed, CD8+ T-cells from HIC were only partially affected by glucose deprivation, while cells from cART were highly glucose-dependent. Importantly, the same difference in glucose dependency was found with SIV-specific CD8+ T-cells from spleen samples of SIV controllers and viremic macaques that strongly differed in their capacity to suppress SIV infection *ex vivo*. This further supports that strict glucose dependency is associated with inefficient HIV/SIV-specific CD8+ T-cells in blood and tissues. Glucose-dependency was observed

for HIV-specific CD8+ T responses from cART individuals but not for CMV-specific CD8+ T-cells, which is in agreement with skewed priming exclusively of HIV-specific CD8+ T-cells rather than a general characteristic of the CD8+ T-cells in these individuals. The glucose dependency of HIV-specific CD8+ T-cells from non-controllers appeared to be associated with dysfunctional (or uncommitted) mitochondria, which could deprive these cells of important metabolic resources. Increased mitochondrial mass has been linked to a survival defect of HIV-specific CD8+ T-cells in non controllers[43], in line with our results. Low mitochondrial membrane potential and high oxidative stress in lymphocytes have also been positively correlated with viral load in untreated HIV-1 infection[44], further supporting the idea that mitochondria dysfunction can negatively impact viral control. Although mitochondrial metabolism is important for the persistence of CD8+ T-cell memory, recent reports indicate that it is not indispensable for memory development[45]. Interestingly, VHL deficiency in CD8+ T-cells increases constitutive levels of HIF1 and glycolytic activity favoring the development of effector memory responses[46]. Although these cells were able to counteract LCMV infection in mice[25], VHL deficiency impaired the formation of terminally differentiated cells. In contrast, VHL-sufficiency in the same model was characterized by the development of central memory responses with increased mitochondrial respiratory capacity[46], which may be critical in the long-term. These results are coherent with our observation that HIV-specific CD8+ T CM cells from HIC and cART individuals were characterized by contrasting differential expression of *VHL* (upregulated in HIC) and *HIF1* (upregulated in cART individuals). The magnitude and polyfunctionality of HIV-specific CD8+ T-cells from HIC was reduced in the presence of menadione, a drug that alters mitochondrial membrane polarization[32]. Menadione can also perturb mitochondrial calcium homeostasis[32], which also affects T-cell activation[47]. In any case, although the number of experiments was limited, CD8+ T-cells from HIC increased oxidative phosphorylation upon contact with infected CD4+ T-cells, further supporting that HIV-specific CD8+ T-cells from HIC had preserved mitochondrial metabolism.

This could be related to the *ID2* upregulation observed in HIC cells. ID2 has been shown to promote effector differentiation and T-cell survival[48], and to reduce mitochondrial damage induced by oxidative stress and to increase survival in cancer cell lines deprived of glucose[49]. CD8+ CM T-cells from HIC showed increased fatty acid uptake. This could indicate that CD8+ CM T-cells from HIC may also rely on fatty acid oxidation, which has been shown to enhance CD8+ T-cell memory generation[29], facilitate the secretion of several effector cytokines[50] and provide superior protection against influenza virus infection[51]. Overall, our results imply that metabolic plasticity, as opposed to strict glucose-dependency, may contribute to the enhanced antiviral capacity of natural HIV controllers' CD8+ T-cells.

To avoid the impact of ongoing viral replication on our analysis, we compared cells from HIC to those from HIV-1-infected individuals on cART. Some nucleoside reverse transcriptase inhibitors (NRTI) can block mitochondrial DNA polymerase gamma function and induce mitochondrial dysfunction[52]. However, not all NRTIs have the same impact on mitochondrial function and the drugs used to treat the individuals whose cells were used in our functional assays are reported to have limited mitochondrial toxicity[52,53] (Supplementary Table 6). The increase in mitochondrial mass is a selective characteristic of HIV-specific CD8+ T-cell responses associated with uncontrolled infection[43]. Moreover, CMV-specific CD8+ T-cell responses from cART individuals did not show glucose dependency. Therefore, impact of antiretroviral treatment does not explain the metabolic defects observed in HIV-specific CD8+ T-cells from cART individuals. In addition, glucose dependency was also found in SIV-specific CD8+ T-cells from ART-naïve SIVmac251 infected macaques with high viremia, showing that this glucose dependency was associated with inefficient HIV/SIV specific CD8+ T-cell responses in subjects with active viral replication or ART-suppressed viremia.

Although glycolysis is a pivotal energy resource for CD8+ T-cell function, tight glucose dependency could impose serious limitations *in vivo*, as already shown in cancer. Tumor cell growth and the tumor microenvironment provoke nutrient restrictions and impair anti-tumoral T-cell effector functions[54]. Similarly, in the context of HIV infection, T-cell activation and homeostasis are accompanied by an increase in T-cell glucose uptake in lymph nodes[55]. HIV-1-infected CD4 T-cells have enhanced glucose uptake and glycolytic activity[34]. Lactic acid, the product of glycolysis, can suppress CD8+ T-cell cytotoxic functions[56]. The glucose dependency of CD8+ T-cells from HIV non-controllers could lead to functional impairment in this glucose-restricted microenvironment. In contrast, the greater metabolic plasticity of cells from HIC would allow them to continue to exert their functions, at least partially, in this setting.

Although, due to the heterogeneity of the data, the interpretation of some differences observed in our study between cells from HIC and cART individuals should be considered with caution, it is worth noting that another recent study showed that dysfunctional HBV-specific CD8+ T-cells are characterized by GLUT1 upregulation and glucose dependency, while functional CMV-specific CD8+ T-cells are able to use oxidative phosphorylation in the absence of glucose[31]. In addition, mitochondria-targeting antioxidant treatment corrected mitochondrial dysfunction and restored HBV-specific T-cell functions[57]. This suggests that limited metabolic plasticity and glucose dependency is a hallmark of dysfunctional antigen-specific CD8+ T-cells.

We show here that HIV/SIV-specific CD8+ T-cell responses from cART individuals or viremic macaques can be reinvigorated by IL-15 pre-treatment. IL-15 induces mitochondrial biogenesis in CD8+ T-cells, to promote the use of fatty acids for energy[29], and enhances the survival and function of HIV-specific CD8+ T-cells[58]. Our results are in agreement with these reports and indicate that these beneficial effects are interrelated. Moreover, our data show that antigen-specific CD8+ T-cells more dependent on glucose, such as HIV-specific CD8+ T-cells, benefited most of the IL-15 mediated enhancement of

447 oxidative metabolism, while the effect was mitigated in cells that were already using mitochondrial
448 respiration to sustain their activity in the absence of glucose, e.g. CMV-specific CD8+ T-cell
449 responses. Importantly, pre-incubation with IL-15 restored non-controllers' CD8+ T-cells' HIV-
450 suppressive capacity *ex vivo,* as previously shown[38]. IL-15 immunotherapy is showing promising
451 results *in vivo* in non-human primate models[59], and this may be related in part to its direct effect on
452 CD8+ T-cell function, as shown here.
453
454 Overall, our findings show that the enhanced functionality of HIV-specific CD8+ T-cells from HIC is
455 imprinted in their memory program and is associated with their ability to use diverse metabolic
456 resources. In contrast, poor functionality of cells from non-controllers is associated with dependency
457 on glycolysis as primary energy source. Our data thus highlight the molecular singularity of HIV-
458 specific CD8+ T-cells from HIC, and point to a metabolic profile compatible with better cell survival
459 and a preserved potential to develop a higher quality anti-HIV effector functions in stressful
460 conditions. Our results indicating that HIV-specific CD8+ T-cell metabolism is linked to control of HIV
461 infection suggest that new pharmacological tools regulating metabolic activity, as explored in the
462 cancer field[60], could help to induce HIV remission and to develop therapeutic vaccines.
463

MATERIALS AND METHODS

Subjects

The HIV controllers (HIC, individuals naïve of antiretroviral treatment and whose last 5 consecutive plasma HIV RNA values were below 400 copies/ml) included in this study belonged to the ANRS CO21 Codex cohort. Strong responders (SR) and weak responders (WR) were defined as HIV controllers whose CD8+ T-cells were able to reduce p24 production by autologous CD4+ T-cells by more and less than 2 logs, respectively (see *Viral Suppression Assay*)[27]. The antiretroviral-treated HIV-infected individuals (cART, antiretroviral treatment for at least 2 years, and undetectable HIV RNA) were part of the ANRS PRIMO cohort or recruited from the outpatients at CHU Kremlin-Bicêtre and CHU Georges Pompidou in Paris. Clinical data for the individuals studied in the single-cell gene expression assays are listed in Supplementary Table 1. Clinical data for the other study participants are summarized in Supplementary Table 5. All participants gave their informed consent and the study was approved by ethics committee (Comité de Protection des Personnes) of Île-de-France XI.

Viral Suppression Assay

The capacity of CD8+ T-cell to suppress HIV-1 infection was analyzed on co-cultures with autologous CD4+ T-cells[61]. After PBMC isolation from peripheral blood by density gradient centrifugation, CD4+ and CD8+ T-cells were separated by, respectively, successive positive and negative magnetic bead sorting (STEMCELL Technologies). CD4+ T-cells were cultured for 3 days in complete RPMI medium in the presence of phytohemagglutinin (1 µg/ml) and interleukin-2 (100 IU/ml). In parallel, CD8+ T-cells were cultured in complete RPMI medium in the absence of stimuli. Activated CD4+ T-cells were infected with HIV-1 Bal by spinoculation for 2 h at 2,000 × g and 22°C[62] and cultured alone or with CD8+ T-cells at a 1:1 ratio for 14 days in interleukin-2 (100 IU/ml)-supplemented complete RPMI. Viral replication was measured in terms of p24 production in the culture supernatants by means of

enzyme-linked immunosorbent assay (XpressBio). In some experiments co-cultures were done in the presence of rapamycin (1 nM, Sigma Aldrich).

For viral suppression assays with CD8+ T-cell subsets, CD4+ and CD8+ T-cells were isolated and cultured as described above. The day of infection, CD8+ T-cells were stained with anti-CD4 FITC (BD), anti-CCR7 PE-Cy7 (eBioscience), anti-CD27-PE (BD) and anti-CD45RA v421 (BD) antibodies. CD8+ T-cell subsets were isolated with a FACSAria III cell sorter (BD). CD8+ T-cell subsets were defined as Naïve (CD4-CD45RA+,CCR7+,CD27+), Central Memory (CD4-CD45RA-,CCR7+,CD27+), Transitional Memory (CD4-CD45RA-,CCR7-,CD27+) or Effector Memory (CD4-CD45RA-,CCR7-,CD27-). After sorting, CD4+ T-cells were challenged with HIV-1 Bal and cultured alone or with the autologous CD8+ T-cell subsets as described above.

Single-Cell Flow Cytometry-assisted Cell Sorting

For each individual twenty million PBMC were thawed and cultured overnight in complete RPMI with 20% FBS. CD8+ T-cells were then separated by magnetic bead sorting (negative selection, STEMCELL Technologies) and stained with the LIVEDEAD Fixable Aqua Dead Cell Stain Kit (Thermo Ficher Scientific), APC-conjugated dextramers (Immudex) and the following antibodies: anti-CD3 AF-700 (BD), CD8 APC-Cy7 (BD), CD45RA v421, CCR7 PE-Cy7 and CD27 PE. For each individual, viable Central Memory CD8+ T-cells were single-cell-sorted (BD FACS ARIA SORP, Becton-Dickinson) in 96-well plates containing the VILO Reaction Mix, SUPERase-In and NP40 (all from Thermo Ficher Scientific). 480 cells were sorted for each group of patients (1440 cells in total). Plates were snap-frozen and stored at -80°C.

Single-Cell Gene Expression

Analysis of gene expression in single cells from the different individuals, in no particular order, was performed as follows. Plates containing sorted single cells were thawed on ice. RNA was denatured

516 at 65°C for 90 seconds and then snap-chilled on ice. An RT mix containing SuperScript Enzyme and T4
517 Gene 32 Protein was then added, followed by RT cycling (25°C: 5 min, 50°C: 30 min, 55°C: 25 min,
518 60°C: 5 min, 70°C: 10 min). Specific target amplification (STA) was performed by adding TaqMan
519 PreAmp Master Mix, 96 Primers mix and EDTA to cDNA, followed by STA cycling (95°C: 10 min, 20
520 cycles of [96°C: 5 s, 60°C 4 min]). The sample was then treated with exonuclease I (New England
521 Biolabs) (37°C: 30 min, 80°C: 15 min).
522
523 Sample pre-mix (SsoFast EvaGreen Supermix with Low ROX (Biorad), DNA Binding Dye (Fluidigm),
524 preamplified Exo 1-treated sample) and Assay mix (Assay Loading Reagent (Fluidigm), Delta Gene
525 primers (Fluidigm)) were loaded on a primed 96.96 Dynamic Array chip (Fluidigm). The chip was
526 transferred into a Biomark (Fluidigm) for thermocycling, and fluorescence was acquired with the GE
527 96×96 PCR+Melt v2 program. For quality control, amplification curves were validated with cDNA
528 from bulk CD8+ T-cells. Linear derivative mode baseline correction was applied. Gene expression
529 values are plotted as Log2Ex, where Log2Ex = LoD – Ct if Ct ≤ LoD (Log2Ex = 0 if Ct > LoD), with LoD =
530 limit of detection (24) and Ct = threshold cycle. A list of genes with raw Ct values is shown in
531 Supplementary Data 1. Cells negative for *CD8, GAPDH* and *ACTB* gene expression were excluded from
532 the analysis.
533
534 **Statistical analyses**
535 The differential gene expression analysis was performed using MAST (Model-based Analysis of Single
536 Cell Transcriptomics) (v1.8.2) packages from R software (v3.5.1). This package is based on the hurdle
537 model, a two-part generalized model for bimodal and/or zero-inflated single cell gene expression
538 data, simultaneously modeling the rate of expression over the background of various transcripts and
539 the positive expression mean [63]. Cells are considered as outliers and removed from the analysis if
540 their total expression (in log2EX) or the number of genes they express are less than two scaled
541 median absolute deviations (MAD) away from the median. The total numbers of cells after data

filtration were as follows: 329 (HIV-controllers, strong responders), 348 (HIV-controllers, weak responders) and 320 (cART-treated individuals).

The hurdle model was applied to each gene in order to detect differentially expressed genes between the groups of interest (HIC [WR and SR], cART,). This model included the group and subject variables as fixed effects, as well as the interaction between group and subject. The last two terms were used to model the pairing between cells from the same subject. To test the difference in expression for each gene, we defined vectors of contrasts and then applied likelihood ratio tests. We obtained p-values that were adjusted according to the Benjamini and Hochberg procedure to control the false discovery rate at 5%[64]. To compare the *between inter-goup* and *intra-group* variance we calculated the F-statistic using one-way ANOVA with Welch correction (v2.4-2).

For t-sne analyses[65] gene expression values (Log2EX, SR and cART groups) of all genes and samples were used.

For additional statistical tests, Graphpad Prism software (GraphPad Software, Inc.) was used. Non parametric Mann-Whitney test was used to compare metabolite uptake and mitochondria mass and to compare the ratio between HIV-specific CD8+ T-cell TNFα responses in medium without and with glucose, between HIV controllers and cART individuals. A non-parametric Wilcoxon paired test was used to compare HIV-specific CD8+ T-cell responses in different conditions.

Metabolite Uptake

Fresh PBMC were stained with anti-CD3 AF 700, anti-CD8 APC-Cy7, CD45RA BV421, CD27 PE, and CCR7 PE-Cy7 (all from BD). Stained samples were then split into three parts and put into contact with 2-NBDG (2-(N-(7-Nitrobenz-2-oxa-1,3-diazol-4-yl)Amino)-2-Deoxyglucose) (150 µM, 30 min) for glucose uptake measurement, BODIPY® 500/510 C1, C12 (4,4-Difluoro-5-Methyl-4-Bora-3a,4a-Diaza-

s-Indacene-3-Dodecanoic Acid) (5 µM, 5 min) for fatty acid uptake measurement, and MitoTracker Green FM (100 nM, 45 min) (all from Thermo Fisher Scientific) for mitochondrial mass measurement (see Supplementary figure 16 for gating strategy). To minimize technical variability, metabolite uptake was compared to the uptake by cells from a reference non-infected individual always analyzed in parallel in each experiment. Metabolite uptake was thus expressed as the relative MFI for cells from each individual when compared to the MFI observed in cells from the reference donor.

Phenotyping

We analyzed by flow cytometry the expression of CCL3, FASL and GZB as markers of antiviral potential, pS6 and pAKT as markers of mTORC1 and mTORC2 activation respectively, and HIF1, (Supplementary Figure 7). Purified PBMC were thawed and rested overnight at 37°C in RPMI medium (RPMI 1640 supplemented with L-glutamine and antibiotics) with 20% heat-inactivated FCS. For cell phenotyping, CD8+ T-cells were separated by magnetic bead sorting (negative selection, STEMCELL Technologies) and stained with the LIVEDEAD Fixable Aqua Dead Cell Stain Kit (Thermo Fischer Scientific), APC-conjugated dextramers (Immudex) and the following antibodies: anti-PD1 BV785, CD45RA BV655, CCR7 Qdot605, CD8 BUV496, CD3 BUV395, CD27 PerCP-Cy5.5 (all from BD Bioscience) and FASL PE-Cy7 (Miltenyi Biotech). Cells were then incubated with PhosFlow Fix buffer, washed with Phosflow Perm-Wash Buffer and stained with anti- CCL3 APC-Cy7 (Miltenyi Biotech), Granzyme B PE-TR BD Bioscience, HIF1a PE (Biolegend), Pospho AKT FITC and pS6 PacBlue/BV421 (both from Cell Signaling). Due to the rarity of HIV-specific CD8+ TCM-cells, the number of events that we could analyze was limited and we could not find significant levels in the expression of CCL3, FASL, pAKT or pS6 in HIV-specific CD8+ TCM-cells ex vivo to allow comparison between cells from HIC and cART individuals. Results for GrZB and HIF1 are depicted in Figure 6.

Intracellular Cytokine Assay

Purified PBMC were thawed and rested overnight at 37°C in RPMI medium (RPMI 1640 supplemented with L-glutamine and antibiotics) with 20% heat-inactivated FCS. For the "No Glucose" condition, cells were rested and stimulated in RPMI without glucose. Cells were then incubated with overlapping peptide pools encompassing HIV-1 consensus subtype B Gag or HCMV pp65 (both obtained through the NIH AIDS Reagent Program, Division of AIDS, NIAID, NIH, cat #12425 and #11549) (2 µg/ml). Anti-CD28/anti-CD49d co-stimulation (1 µL/mL) and the anti-CD107α marker were used in each condition. Phorbol myristate acetate (80 ng/mL) together with ionomycin (1 µg/mL; Sigma-Aldrich) was used as positive control. Golgi stop (1 µg/mL; BD Biosciences) and Brefeldin A (10 µg/mL; Sigma-Aldrich) were added 30 min after the start of all incubations. Cells were then stained with the LIVE/DEAD Fixable Aqua Dead Cell Stain kit (Thermo Fisher Scientific), and with anti-CD3 and anti-CD8 antibodies. BD Cytofix/Cytoperm™ (BD Biosciences) was used for cell permeabilization prior to staining for intracellular markers. Intracellular staining used anti-IFNγ, anti-IL-2 and anti-TNFα (see Supplementary Figure 17 for gating strategy). In some experiments cells were fixed with permeabilized with Phosflow fix/perm buffers (BD Bioscience) and cells were stained for intracellular IFNγ, TNFα, pS6 and pAKT as above. Menadione sodium bisulfite (Sigma-Aldrich) was used at 5 µM.

Measurement of oxygen consumption rate

Oxygen consumption rate (OCR) and extracellular acidification rate (ECAR) were measured using a Seahorse XF96 metabolic analyser as indicated by the manufacturer (Seahorse XF Technology, Agilent). CD8+ T-cells (2× 10^5 cells per well) were seeded on XF96 plates (Agilent Seahorse) pre-coated with 0.5 mg/ml Cell Tack (Corning). Cells were incubated for 50 min in a CO2-free incubator at 37°C before loading the plate in the Seahorse analyser. Oligomycin (2.5 µM), FCCP (0.9 µM) 4) and Rotenone/antimycin A (1 µM each) were sequentially added to the cells and OCR was monitored overtime. The maximal respiratory capacity is calculated as the OCR after FCCP addition subtracted the OCR after oligomycin. For glycolysis (ECAR), cells were cultured in the absence of glucose and

then XFmedia, glucose (10 mM), oligomycin (2.65 µM), and 2-DG (100 mM)) were sequentially added to the cells.

In some experiments OCR and ECAR were analyzed in CD8+ T-cells from HIC after co-culture with HIV-infected or non-infected autologous CD4+ T-cells. Briefly, CD4+ T-cells from HIC were or not infected in vitro with HIV-1 BaL as described above. After three days, cells were washed and autologous CD8+ T-cells were added to the cultures of non-infected and infected CD4+ T-cells at a 1:1 ratio. Four days later, CD8+ T-cells were isolated again from the co-culture (flow sorted based on viability and expression of CD8) and their metabolic activity analyzed with the Seahorse XF96 analyser.

Studies with cells from SIVmac251 infected Cynomolgus macaques

Adult male cynomolgus macaques (*Macaca fascicularis*) were imported from Mauritius and housed in the facilities of the "Commissariat à l'Energie Atomique et aux Energies Alternatives" (CEA, Fontenay-aux-Roses, France). All animals studied here were part of the ANRS SIC and ANRS pVISCONTI studies and were inoculated (viral doses ranging from 5 to 1000 AID_{50}) with the same batch of uncloned SIVmac251 (provided by A. M. Aubertin, Université Louis Pasteur, Strasbourg, France). Cells used were obtained during necropsies of animals at the chronic phase of infection (between 8 and 18 months post-infection). Peripheral blood was collected by venous puncture into BD Vacutainer Plus Plastic K3EDTA tubes or BD Vacutainer CPT Mononuclear Cell Preparation Tube - Sodium Heparin (BD Biosciences). Spleen and lymph nodes were processed by mechanical disruption in RPMI media using a GentleMACS dissociator (Miltenyi Biotech), followed by gradient in Lymphocyte separation medium and red cell lysis.

Viral load

644 Plasma viremia was determined using quantitative real time PCR with sensitivity of 12.3 copies/mL.
645 Viral RNA was prepared from 100 µl of cell-free plasma, using the NucleoSpin 96 Virus core kit
646 (Macherey-Nagel SARL, Hoerdt, France) under vacuum, according to the manufacturer's instructions.
647 RNA was eluted in 100 µl of nuclease-free water and frozen immediately at −80°C until analysis.
648 SIVmac251 virus diluted in and EDTA-treated plasma samples from macaques not infected with SIV
649 was used to generate a standard curve (serial 10-fold dilutions). Three titrated SIVmac251-infected
650 EDTA-treated plasma samples and two EDTA-treated plasma samples from SIV-negative macaques
651 were used as positive and negative reverse transcription-PCR controls, respectively. Standards,
652 controls, and viral RNA samples were extracted and tested in parallel under the same conditions. The
653 SIVmac251 gag cDNA sequence, ligated into the plasmid pCR2-TOPO (Invitrogen), was used as a
654 positive control for PCR.
655
656 Quantitative RT-PCR was performed with a SuperScript III Platinum One-Step qRT-PCR Kit
657 (Thermofisher) in a CFX96 Touch Real-Time PCR Detection System (BioRad) under the following
658 conditions: 12.5 µl of 2X reaction mixture, 0.5 µl of RNaseOUT (40U/µl), 0.5 µl of Superscript III
659 reverse transcriptase/Platinum,Taq DNA Polymerase, 1 µl of each primer (125 µM), 0.5 µl of the
660 fluorogenic probe (135 µM), and 10-µl of RNA elution samples. The probe and primers were designed
661 to amplify a region of SIVmac251 gag[66]. Forward primer was 5'-GCAGAGGAGGAAATTACCCAGTAC-3'
662 (24 bp) and reverse primer was 5'-CAATTTTACCCAGGCATTTAATGTT-3' (25 bp). The TaqMan probe
663 sequence was 5'-FAM-TGTCCACCTGCCATTAAGCCCGA-BHQ1-3' (23 bp). This probe had a fluorescent
664 reporter dye, FAM (6-carboxyfluorescein), attached to its 5' end and the quencher BHQ1 (Black Hole
665 Quencher 1) attached to its 3' end. Samples were heated for 30 min at 56°C and 5 min at 95°C,
666 followed by 50 cycles of 95°C for 15 s and 60°C for 1 min.
667
668 *Intracellular cytokine staining*

669 Splenocytes were thawed, resuspended at 1 × 10^6/mL in R20 media and kept at 37°C overnight. Cells
670 were then stimulated with 2 µg/mL of SIV peptide pools in the presence of costimulatory monoclonal
671 antibodies anti-CD28 (clone L293) and anti-CD49d (clone 9F10) at 1 µg/mL and stained with anti-
672 CD107a for 30 minutes. Golgi Stop (BD Biosciences) and brefeldin A (BFA, 5 µg/mL; Sigma) were then
673 added. A pool containing 24 optimal peptides (ProImmune) was used to assess SIV-specific CD8+ T
674 cell responses. Co-stimulatory antibodies + Golgi Stop + BFA alone were used as a negative control.
675 Cells were incubated for a total of 6 hours and stained to assess cytokine production by SIV-specific
676 cells. After washing, cells were surface stained with anti-CD3, CD4 and CD8 antibodies. Cells were
677 then permeabilized (Cytofix/CytoPerm kit; BD Biosciences) and stained for IFNg, TNFa, IL-2 and
678 Perforin. The following antibodies were used: CD107a – V450 (clone H4A3, BD), CD3 – AF700 (clone
679 SP34-2, BD), CD4 – PerCP Cy5.5 (clone L200, BD), CD8a – APC-Cy7 (clone RPA-T8, BD), IFNg – PE-Cy7
680 (clone B27, BD), IL-2 – PE (clone MQ1-17H12, BD), TNFa – PE-CF594 (clone Mab11, BD) and Perforin –
681 FITC (clone Pf-344, Mabtech). Flow cytometry was performed with an LSRII instrument (BD
682 Biosciences), and data were analyzed with FlowJo V.10 software (TreeStar Inc.).
683
684 *CD8 T cell suppression assay*
685 CD4+ and CD8+ T cells were purified from PBMCs or tissues cell suspensions with antibody-coated
686 magnetic beads in a Robosep instrument (Stemcell Technologies). Custom non-human primate
687 selection kits (Stemcell Technologies) were used to purify CD4+ T-cells (positive selection) and CD8+ T
688 cells (negative selection). The capacity of CD8+ T cells to suppress SIV infection of autologous CD4+ T
689 cells[67] was adapted from the assay with human cells described above. CD4+ cells were stimulated for
690 3 days with 5µg/mL Concanavalin A (ConA) in the presence of IL-2 (Miltenyi Biotec) at 100 IU/mL.
691 CD8+ T cells were kept in culture in the absence of any mitogen or cytokine or pre-incubated with IL-
692 15. CD4+ T cells were then superinfected with $SIVmac_{251}$ (MOI = 10^{-3}) in the presence or absence of
693 CD8+ T cells (ratio CD4:CD8 of 1:1). Cells were cultured for 14 days in R10 medium containing IL-2

694 (100 IU/mL). Viral replication was monitored by p27 detection in culture supernatants (XpressBio) at
695 day 7.
696
697 *Ethics statement*
698 Non-human primates (NHP, which includes *M. fascicularis*) are used at the CEA in accordance with
699 French national regulations and under the supervision of national veterinary inspectors (CEA Permit
700 Number A 92-032-02). The CEA complies with the Standards for Human Care and Use of Laboratory
701 Animals of the Office for Laboratory Animal Welfare (OLAW, USA) under OLAW Assurance number
702 #A5826-01. All experimental procedures were conducted according to European Directive 2010/63
703 (recommendation number 9) on the protection of animals used for scientific purposes and national
704 regulations.
705
706 The SIC and pVISCONTI studies were accredited under statement number 13–005, by the ethics
707 committee "Comité d'Ethique en Expérimentation Animale du CEA" registered and authorized under
708 numbers 01114.01 and 2453-2015102713323361v2 by the French Ministry of Education and
709 Research. The animals were used under the supervision of the veterinarians in charge of the animal
710 facility and were housed under controlled conditions of humidity, temperature, and light (12-hour
711 light/12-hour dark cycles). Water was available ad libitum. Animals were monitored and fed
712 commercial monkey chow and fruit 1-2 times daily by trained personnel. The macaques
713 were provided with environmental enrichment, including toys, novel foodstuffs, and music, under
714 the supervision of the CEA Animal Welfare Body.
715
716 Animals were sedated by intra-muscular injection of 10 mg/kg ketamine (Rhone-Merieux, Lyon,
717 France) euthanized by intravenous injection of sodium pentobarbital (200 mg/Kg) and tissue
718 samples were immediately collected during autopsia.
719

Reporting Summary

Further information on research design is available in the Nature Research Reporting Summary linked to this article.

DATA AVAILABILITY

All data generated or analyzed during this study are available from the corresponding author upon request. Gene expression data are included in this article and its supplementary information files..

ACKNOWLEDGEMENTS

The authors wish to thank A Tadesse, S Hendou, A Essat, C Jung and K Bourdic for help with inclusion of HIV-infected individuals. The authors wish to thank D Desjardin and N Bosquet for help with the macaque studies. The authors especially thank the investigators, clinical personal and HIV-infected individuals participating in the ANRS CO6 PRIMO and the ANRS CO21 cohorts for their cooperation. The authors thank the Cytometry and Biomarkers UTechS plate-form at Institut Pasteur and the personnel from the "Infectious Disease Models and Innovative Therapies (IDMIT) plate-form for technical support. D Young, a medical English editor supported with funds from AS-C laboratory, provided English editorial assistance to the authors during preparation of this manuscript.

This study was conducted with funds from the French National Agency for Research on AIDS and Viral Hepatitis (ANRS), MSDAVENIR and from the European Union (EU)'s Horizon 2020 research and innovation programme under the Marie Sklodowska-Curie grant agreement No 706871. MA received support from EU (grant 706871) and complementary support from Sidaction. CP received support from ANRS. JCV-C received support from Institut Pasteur through the Roux-Cantarini program. The ANRS CO6 and CO21 cohorts are sponsored and funded by the ANRS. IDMIT infrastructure was supported by the French government "Programme d'Investissements d'Avenir" (PIA) under Grant ANR-11-INBS-0008.

AUTHOR CONTRIBUTIONS

M.A., C.P., C.L., V.M., JCV-C, performed experiments; M.A., S.V., M-A.D., and A.S-C. analyzed the data; L.W., C.G., L.M., F.B. and O.L. contributed to inclusion of study participants, obtaining and validation of clinical information; C.P., B.V., R.L.G. and AS-C contributed to the design and development of the macaque study; G.P., MM-T, O.L. and AS-C contributed to the conception of the study; M.A., O.L. and AS-C designed the study; M.A. and AS-C drafted the article; all authors critically reviewed the manuscript.

COMPETING FINANCIAL INTERESTS

The authors declare no competing financial interests

REFERENCES

1 Walker, B. & McMichael, A. The T-Cell Response to HIV. *Cold Spring Harbor Perspectives in Medicine* **2**, a007054, doi:10.1101/cshperspect.a007054 (2012).

2 Appay, V. *et al.* Dynamics of T Cell Responses in HIV Infection. *The Journal of Immunology* **168**, 3660-3666, doi:10.4049/jimmunol.168.7.3660 (2002).

3 Takata, H. *et al.* Delayed differentiation of potent effector CD8+ T cells reducing viremia and reservoir seeding in acute HIV infection. *Sci Transl Med* **9**, doi:10.1126/scitranslmed.aag1809 (2017).

4 Migueles, S. A. *et al.* HIV-specific CD8+ T cell proliferation is coupled to perforin expression and is maintained in nonprogressors. *Nat Immunol* **3**, 1061-1068, doi:10.1038/ni845 (2002).

5 Betts, M. R. *et al.* HIV nonprogressors preferentially maintain highly functional HIV-specific CD8+ T cells. *Blood* **107**, 4781-4789, doi:10.1182/blood-2005-12-4818 (2006).

6 Migueles, S. A. *et al.* Lytic granule loading of CD8+ T cells is required for HIV-infected cell elimination associated with immune control. *Immunity* **29**, 1009-1021, doi:10.1016/j.immuni.2008.10.010 (2008).

7 Saez-Cirion, A. & Pancino, G. HIV controllers: a genetically determined or inducible phenotype? *Immunol Rev* **254**, 281-294, doi:10.1111/imr.12076 (2013).

8 Saez-Cirion, A. *et al.* HIV controllers exhibit potent CD8 T cell capacity to suppress HIV infection ex vivo and peculiar cytotoxic T lymphocyte activation phenotype. *Proc Natl Acad Sci U S A* **104**, 6776-6781, doi:10.1073/pnas.0611244104 (2007).

9 Angin, M. *et al.* Preservation of Lymphopoietic Potential and Virus Suppressive Capacity by CD8+ T Cells in HIV-2-Infected Controllers. *J Immunol* **197**, 2787-2795, doi:10.4049/jimmunol.1600693 (2016).

10 Lecuroux, C. *et al.* CD8 T-cells from most HIV-infected patients lack ex vivo HIV-suppressive capacity during acute and early infection. *PLoS One* **8**, e59767, doi:10.1371/journal.pone.0059767 (2013).

11 Tansiri, Y., Rowland-Jones, S. L., Ananworanich, J. & Hansasuta, P. Clinical outcome of HIV viraemic controllers and noncontrollers with normal CD4 counts is exclusively determined by antigen-specific CD8+ T-cell-mediated HIV suppression. *PLoS One* **10**, e0118871, doi:10.1371/journal.pone.0118871 (2015).

12 Buckheit, R. W., 3rd, Salgado, M., Silciano, R. F. & Blankson, J. N. Inhibitory potential of subpopulations of CD8+ T cells in HIV-1-infected elite suppressors. *J Virol* **86**, 13679-13688, doi:10.1128/JVI.02439-12 (2012).

13 Sallusto, F., Geginat, J. & Lanzavecchia, A. Central memory and effector memory T cell subsets: function, generation, and maintenance. *Annu Rev Immunol* **22**, 745-763, doi:10.1146/annurev.immunol.22.012703.104702 (2004).

14 Burgers, W. A. *et al.* Association of HIV-specific and total CD8+ T memory phenotypes in subtype C HIV-1 infection with viral set point. *J Immunol* **182**, 4751-4761, doi:10.4049/jimmunol.0803801 (2009).

15 Ladell, K. *et al.* Central memory CD8+ T cells appear to have a shorter lifespan and reduced abundance as a function of HIV disease progression. *J Immunol* **180**, 7907-7918 (2008).

16 Geginat, J., Lanzavecchia, A. & Sallusto, F. Proliferation and differentiation potential of human CD8+ memory T-cell subsets in response to antigen or homeostatic cytokines. *Blood* **101**, 4260-4266, doi:10.1182/blood-2002-11-3577 (2003).
17 Flatz, L. *et al.* Single-cell gene-expression profiling reveals qualitatively distinct CD8 T cells elicited by different gene-based vaccines. *Proc Natl Acad Sci U S A* **108**, 5724-5729, doi:10.1073/pnas.1013084108 (2011).
18 Saez-Cirion, A. *et al.* Heterogeneity in HIV suppression by CD8 T cells from HIV controllers: association with Gag-specific CD8 T cell responses. *J Immunol* **182**, 7828-7837, doi:10.4049/jimmunol.0803928 (2009).
19 Cocchi, F. *et al.* Identification of RANTES, MIP-1 alpha, and MIP-1 beta as the major HIV-suppressive factors produced by CD8+ T cells. *Science* **270**, 1811-1815 (1995).
20 Phan, A. T. & Goldrath, A. W. Hypoxia-inducible factors regulate T cell metabolism and function. *Mol Immunol* **68**, 527-535, doi:10.1016/j.molimm.2015.08.004 (2015).
21 Pollizzi, K. N. *et al.* Asymmetric inheritance of mTORC1 kinase activity during division dictates CD8(+) T cell differentiation. *Nat Immunol* **17**, 704-711, doi:10.1038/ni.3438 (2016).
22 Pollizzi, K. N. *et al.* mTORC1 and mTORC2 selectively regulate CD8(+) T cell differentiation. *J Clin Invest* **125**, 2090-2108, doi:10.1172/JCI77746 (2015).
23 Hung, C. M., Garcia-Haro, L., Sparks, C. A. & Guertin, D. A. mTOR-dependent cell survival mechanisms. *Cold Spring Harb Perspect Biol* **4**, doi:10.1101/cshperspect.a008771 (2012).
24 Maxwell, P. H. *et al.* The tumour suppressor protein VHL targets hypoxia-inducible factors for oxygen-dependent proteolysis. *Nature* **399**, 271-275, doi:10.1038/20459 (1999).
25 Doedens, A. L. *et al.* Hypoxia-inducible factors enhance the effector responses of CD8(+) T cells to persistent antigen. *Nat Immunol* **14**, 1173-1182, doi:10.1038/ni.2714 (2013).
26 Ruschke, K. *et al.* Repin1 maybe involved in the regulation of cell size and glucose transport in adipocytes. *Biochemical and biophysical research communications* **400**, 246-251, doi:10.1016/j.bbrc.2010.08.049 (2010).
27 Lecuroux, C. *et al.* Both HLA-B*57 and plasma HIV RNA levels contribute to the HIV-specific CD8+ T cell response in HIV controllers. *J Virol* **88**, 176-187, doi:10.1128/JVI.02098-13 (2014).
28 Ndhlovu, Z. M. *et al.* Elite controllers with low to absent effector CD8+ T cell responses maintain highly functional, broadly directed central memory responses. *J Virol* **86**, 6959-6969, doi:10.1128/JVI.00531-12 (2012).
29 van der Windt, G. J. & Pearce, E. L. Metabolic switching and fuel choice during T-cell differentiation and memory development. *Immunol Rev* **249**, 27-42, doi:10.1111/j.1600-065X.2012.01150.x (2012).
30 Henson, S. M. *et al.* p38 signaling inhibits mTORC1-independent autophagy in senescent human CD8(+) T cells. *J Clin Invest* **124**, 4004-4016, doi:10.1172/JCI75051 (2014).
31 Schurich, A. *et al.* Distinct Metabolic Requirements of Exhausted and Functional Virus-Specific CD8 T Cells in the Same Host. *Cell Rep* **16**, 1243-1252, doi:10.1016/j.celrep.2016.06.078 (2016).

32 Gerasimenko, J. V. *et al.* Menadione-induced apoptosis: roles of cytosolic Ca(2+) elevations and the mitochondrial permeability transition pore. *J Cell Sci* **115**, 485-497 (2002).
33 Freeman, G. J., Wherry, E. J., Ahmed, R. & Sharpe, A. H. Reinvigorating exhausted HIV-specific T cells via PD-1-PD-1 ligand blockade. *J Exp Med* **203**, 2223-2227, doi:10.1084/jem.20061800 (2006).
34 Valle-Casuso, J. C. *et al.* Cellular Metabolism Is a Major Determinant of HIV-1 Reservoir Seeding in CD4(+) T Cells and Offers an Opportunity to Tackle Infection. *Cell metabolism* **29**, 611-626 e615, doi:10.1016/j.cmet.2018.11.015 (2019).
35 Planas, D. *et al.* HIV-1 selectively targets gut-homing CCR6+CD4+ T cells via mTOR-dependent mechanisms. *JCI Insight* **2**, doi:10.1172/jci.insight.93230 (2017).
36 Donnelly, R. P. *et al.* mTORC1-dependent metabolic reprogramming is a prerequisite for NK cell effector function. *J Immunol* **193**, 4477-4484, doi:10.4049/jimmunol.1401558 (2014).
37 Petrovas, C. *et al.* HIV-specific CD8+ T cells exhibit markedly reduced levels of Bcl-2 and Bcl-xL. *J Immunol* **172**, 4444-4453 (2004).
38 Shasha, D. *et al.* Elite controller CD8+ T cells exhibit comparable viral inhibition capacity, but better sustained effector properties compared to chronic progressors. *J Leukoc Biol* **100**, 1425-1433, doi:10.1189/jlb.4A0915-422R (2016).
39 Gautam, S. *et al.* The transcription factor c-Myb regulates CD8(+) T cell stemness and antitumor immunity. *Nat Immunol* **20**, 337-349, doi:10.1038/s41590-018-0311-z (2019).
40 Doering, T. A. *et al.* Network analysis reveals centrally connected genes and pathways involved in CD8+ T cell exhaustion versus memory. *Immunity* **37**, 1130-1144, doi:10.1016/j.immuni.2012.08.021 (2012).
41 Pauken, K. E. *et al.* Epigenetic stability of exhausted T cells limits durability of reinvigoration by PD-1 blockade. *Science* **354**, 1160-1165, doi:10.1126/science.aaf2807 (2016).
42 Noel, N. *et al.* Long-Term Spontaneous Control of HIV-1 Is Related to Low Frequency of Infected Cells and Inefficient Viral Reactivation. *J Virol* **90**, 6148-6158, doi:10.1128/JVI.00419-16 (2016).
43 Petrovas, C. *et al.* Increased mitochondrial mass characterizes the survival defect of HIV-specific CD8(+) T cells. *Blood* **109**, 2505-2513, doi:10.1182/blood-2006-05-021626 (2007).
44 Perrin, S. *et al.* HIV-1 infection and first line ART induced differential responses in mitochondria from blood lymphocytes and monocytes: the ANRS EP45 "Aging" study. *PLoS One* **7**, e41129, doi:10.1371/journal.pone.0041129 (2012).
45 Raud, B., McGuire, P. J., Jones, R. G., Sparwasser, T. & Berod, L. Fatty acid metabolism in CD8(+) T cell memory: Challenging current concepts. *Immunol Rev* **283**, 213-231, doi:10.1111/imr.12655 (2018).
46 Phan, A. T. *et al.* Constitutive Glycolytic Metabolism Supports CD8(+) T Cell Effector Memory Differentiation during Viral Infection. *Immunity* **45**, 1024-1037, doi:10.1016/j.immuni.2016.10.017 (2016).
47 Quintana, A. *et al.* T cell activation requires mitochondrial translocation to the immunological synapse. *Proc Natl Acad Sci U S A* **104**, 14418-14423, doi:10.1073/pnas.0703126104 (2007).

48 Cannarile, M. A. *et al.* Transcriptional regulator Id2 mediates CD8+ T cell immunity. *Nat Immunol* **7**, 1317-1325, doi:10.1038/ni1403 (2006).

49 Zhang, Z., Rahme, G. J., Chatterjee, P. D., Havrda, M. C. & Israel, M. A. ID2 promotes survival of glioblastoma cells during metabolic stress by regulating mitochondrial function. *Cell Death Dis* **8**, e2615, doi:10.1038/cddis.2017.14 (2017).

50 de Jong, A. J., Kloppenburg, M., Toes, R. E. & Ioan-Facsinay, A. Fatty acids, lipid mediators, and T-cell function. *Front Immunol* **5**, 483, doi:10.3389/fimmu.2014.00483 (2014).

51 Champagne, D. P. *et al.* Fine-Tuning of CD8(+) T Cell Mitochondrial Metabolism by the Respiratory Chain Repressor MCJ Dictates Protection to Influenza Virus. *Immunity* **44**, 1299-1311, doi:10.1016/j.immuni.2016.02.018 (2016).

52 Gardner, K., Hall, P. A., Chinnery, P. F. & Payne, B. A. HIV treatment and associated mitochondrial pathology: review of 25 years of in vitro, animal, and human studies. *Toxicol Pathol* **42**, 811-822, doi:10.1177/0192623313503519 (2014).

53 Margolis, A. M., Heverling, H., Pham, P. A. & Stolbach, A. A review of the toxicity of HIV medications. *J Med Toxicol* **10**, 26-39, doi:10.1007/s13181-013-0325-8 (2014).

54 Siska, P. J. & Rathmell, J. C. T cell metabolic fitness in antitumor immunity. *Trends Immunol* **36**, 257-264, doi:10.1016/j.it.2015.02.007 (2015).

55 Sathekge, M., Maes, A., Kgomo, M. & Van de Wiele, C. Fluorodeoxyglucose uptake by lymph nodes of HIV patients is inversely related to CD4 cell count. *Nucl Med Commun* **31**, 137-140, doi:10.1097/MNM.0b013e3283331114 (2010).

56 Fischer, K. *et al.* Inhibitory effect of tumor cell-derived lactic acid on human T cells. *Blood* **109**, 3812-3819, doi:10.1182/blood-2006-07-035972 (2007).

57 Fisicaro, P. *et al.* Targeting mitochondrial dysfunction can restore antiviral activity of exhausted HBV-specific CD8 T cells in chronic hepatitis B. *Nat Med*, doi:10.1038/nm.4275 (2017).

58 Mueller, Y. M. *et al.* IL-15 enhances survival and function of HIV-specific CD8+ T cells. *Blood* **101**, 1024-1029, doi:10.1182/blood-2002-07-1957 (2003).

59 Watson, D. C. *et al.* Treatment with native heterodimeric IL-15 increases cytotoxic lymphocytes and reduces SHIV RNA in lymph nodes. *PLoS Pathog* **14**, e1006902, doi:10.1371/journal.ppat.1006902 (2018).

60 Chang, C. H. & Pearce, E. L. Emerging concepts of T cell metabolism as a target of immunotherapy. *Nat Immunol* **17**, 364-368, doi:10.1038/ni.3415 (2016).

61 Saez-Cirion, A., Shin, S. Y., Versmisse, P., Barre-Sinoussi, F. & Pancino, G. Ex vivo T cell-based HIV suppression assay to evaluate HIV-specific CD8+ T-cell responses. *Nat Protoc* **5**, 1033-1041, doi:10.1038/nprot.2010.73 (2010).

62 O'Doherty, U., Swiggard, W. J. & Malim, M. H. Human immunodeficiency virus type 1 spinoculation enhances infection through virus binding. *J Virol* **74**, 10074-10080, doi:10.1128/jvi.74.21.10074-10080.2000 (2000).

63 Finak, G. *et al.* MAST: a flexible statistical framework for assessing transcriptional changes and characterizing heterogeneity in single-cell RNA sequencing data. *Genome biology* **16**, 278, doi:10.1186/s13059-015-0844-5 (2015).

64 Benjamini, Y. & Hochberg, Y. Controlling the False Discovery Rate: A Practical and Powerful Approach to Multiple Testing. *Journal of the Royal Statistical Society. Series B (Methodological)* **57**, 189-300 (1995).

65 van der Maaten, L. & Hinton, G. Visualizing Data using t-SNE. *J. Mach. Learn. Res.* **9**, 2579-2605 (2008).

66 Hofmann-Lehmann, R. *et al.* Sensitive and robust one-tube real-time reverse transcriptase-polymerase chain reaction to quantify SIV RNA load: comparison of one- versus two-enzyme systems. *AIDS Res Hum Retroviruses* **16**, 1247-1257, doi:10.1089/08892220050117014 (2000).
67 Bruel, T. *et al.* Long-term control of simian immunodeficiency virus (SIV) in cynomolgus macaques not associated with efficient SIV-specific CD8+ T-cell responses. *J Virol* **89**, 3542-3556, doi:10.1128/JVI.03723-14 (2015).

958

959 **FIGURE LEGENDS**

960 **Figure 1**

961 a) Representative examples of viral suppression assays, as previously shown[8,18]. Gag p24
962 concentrations in supernatants from HIV-infected CD4+ T cells alone (green squares and lines) and
963 CD4+/CD8+ T cell co-cultures (orange triangles and lines), using cells isolated from an HIV controller
964 (left) and an antiretroviral-treated individual (right) on different days of culture after HIV challenge.
965 0.1 ng/ml is considered as the lower limit of detection in our p24 ELISA. Data are means and standard
966 deviation of three replicates. b) Gag p24 concentrations in supernatants from HIV-infected CD4+ T
967 cells alone (green column) isolated from an HIV controller (top) or a cART-individual (bottom), in co-
968 culture with bulk or flow-cytometry-sorted CD8+ T cell subsets on day 7 post-challenge (orange
969 columns; N: Naïve, CM: Central Memory, TM: Transitional Memory, EM: Effector Memory). Mean
970 and values for 3 replicates are shown. Representative results of independent experiments with cells
971 from 3 HIV controllers and 3 cART-individuals. c) Median percentage CD38/HLADR activation marker
972 expression by flow-sorted HIV-specific viable central memory CD8+ T cells isolated from HIV
973 controllers (n=5 individuals) and cART (n=5 individuals). d) T-sne analyses of gene expression by flow-
974 sorted HIV-specific central memory CD8+ T cells from HIV controllers (red circles) (n=329 cells) and
975 cART individuals (blue circles) (n=320 cells).

976

977 **Figure 2**

978 Differentially expressed genes linked to CD8+ T cells effector functions in HIV-specific central
979 memory CD8+ T cells from HIV controllers (red) and cART individuals (blue). Violin plots represent
980 gene expression as Log2ex (limit of detection – threshold cycle) for each cell after data filtration. Cells
981 negative for CD8, GAPDH and ACTB or considered as outliers (if their total expression (in log2EX) or
982 the number of genes they express are less than two scaled median absolute deviations away from
983 the median) were excluded from the analyses. Values for each single cell analyzed (n=329 cells for

HIC, and n=320 cells for cART) are represented as scatter dots. The width of the plots represents the kernel probability density of events at each given value. The proportion of cells lacking expression of a gene is represented by the wideness of the base of the violin plots. The hurdle model was applied to each gene in order to detect differentially expressed genes between cells from HIC and cART individuals. For all genes depicted a statistical significant difference ($p<0.05$ after adjustment according to the Benjamini and Hochberg procedure to control the false discovery rate at 5%) in either continuous, discrete or hurdle analyses was found. Red or blue color of the P values indicate higher expression in cells from HIC or cART individuals respectively.

Figure 3

Genes differentially expressed by HIV-specific central memory CD8+ T cells from HIV controllers (red) and cART individuals (blue). Violin plots represent gene expression as Log2ex (limit of detection – threshold cycle) for each cell after data filtration. Cells negative for CD8, GAPDH and ACTB or considered as outliers (if their total expression (in log2EX) or the number of genes they express are less than two scaled median absolute deviations away from the median) were excluded from the analyses. Values for each single cell analyzed (n=329 cells for HIC, and n=320 cells for cART) are represented as scatter dots. The width of the plots represents the kernel probability density of events at each given value. The proportion of cells lacking expression of a gene is represented by the wideness of the base of the violin plots. The hurdle model was applied to each gene in order to detect differentially expressed genes between cells from HIC and cART individuals. For all genes depicted a statistical significant difference ($p<0.05$ after adjustment according to the Benjamini and Hochberg procedure to control the false discovery rate at 5%) in either continuous, discrete or hurdle analyses was found. Red or blue colors of the P values indicate higher expression in cells from HIC or cART individuals respectively. (A) Genes upreglated in cells from cART individuals. (B) Genes upregulated in cells from HIV controllers.

Figure 4

A) Gene expression t-SNE plots. The first plot (top left) shows single cells from HIV controllers (n=329 cells) (red) and cART (n=320 cells) (blue) individuals. The remaining dot plots are colored on the basis of gene expression values. Groups of neighbor cells identified by the t-sne analysis enriched (>90%) in cells from HIV controllers (red) and cART individuals (blue) are indicated for visual reference. B) Heat map of genes differentially expressed (filtered based on the coefficient of the hurdle analysis) in cells from HIV controllers (red) and cART individuals (blue). Cells are ordered based on the first axis of the t-sne analyses.

Figure 5

(a) T-sne analysis of gene expression by cells from HIC strong responders (n=329 cells) (red), HIC weak responders (n=348 cells) (green) and cART individuals (n=320 cells) (blue). (b-d) Genes differentially expressed by HIV-specific central memory CD8+ T cells from HIV controllers (strong (red) and weak (orange) responders) and cART individuals (blue). Violin plots represent gene expression as Log2ex (limit of detection – threshold cycle) for each cell after data filtration. Cells negative for CD8, GAPDH and ACTB or considered as outliers (if their total expression (in log2EX) or the number of genes they express are less than two scaled median absolute deviations away from the median) were excluded from the analyses. Values for each single cell analyzed (n=329 cells for HIC SR, n=348 cells for HIC WR and n=320 cells for cART) are represented as scatter dots. The width of the plots represents the kernel probability density of events at each given value. The proportion of cells lacking expression of a gene is represented by the wideness of the base of the violin plots. The hurdle model was applied to each gene in order to detect differentially expressed genes between cells from HIC SR, WR and cART individuals. For all genes depicted a statistical significant difference ($p<0.05$ after adjustment according to the Benjamini and Hochberg procedure to control the false discovery rate at 5%) in either continuous, discrete or hurdle analyses was found. Genes upregulated

in cells from HIC WR are in orange, genes upregulated in cells from HIC WR are in red; genes upregulated in cells from cART individuals are in blue.

Figure 6

A) Percentage of cells carrying high levels of GrZB (left) and expression levels (median fluorescence intensity, MFI) of HIF1α among HIV-specific CD8+ T CM cells from HIC (n=10 individuals) and cART (n=7 individuals) as determined by flow cytometry. B) Flow cytometry analyses of fatty acid (BODIPY) and glucose (NBDG) uptake by central memory CD8+ T cells from cART (blue circles, n=11 individuals) and HIV controllers (red circles, n=10 individuals). Results are expressed as the relative MFI compared to the MFI (set as 100) obtained with reference cells from a non-infected donor, which were analyzed in parallel for each experiment. The ratio of fatty acid vs glucose uptake for each individuals is also shown (right panel). (A,B) A non-parametric two-tailed Mann-Whitney test was used to compare differences between the groups. Each symbol represents values for cells from one individual. Medians are represented as horizontal lines.

Figure 7

a) TNFα production and total response (sum of TNFα, IFNγ, CD107a and IL2 production) by HIV-specific CD8+ T cells from HIV controllers (n=11 individuals, red symbols) and cART (n=8 individuals, blue symbols, [two individuals, 670115 and 350108, did not show TNFa responses above background in any conditions]) against a pool of HIV-Gag peptides in control medium, in medium without glucose and in the presence of menadione. The ratio "without/with glucose" represents the ratio between HIV-specific CD8+ T cell TNFα responses in medium without and with glucose, for HIC controllers (red symbols) and cART individuals (blue symbols), (b) Polyfunctional responses (3 or 4 functions; i.e. co-expression of TNFα, IFNγ, CD107a, or IL2) against a pool of HIV-Gag peptides by HIV-specific CD8+ T cells from HIV controllers (n=11 individuals, red symbols) and cART individuals (n=9 individuals, blue symbols, excluding 670115 with no Total HIV response) in control medium, in medium without

glucose, and in the presence of menadione. (a,b) Each symbol represents values for cells from one individual. Medians are represented as horizontal lines. A non-parametric two-tailed Wilcoxon paired test was used to compare HIV-specific CD8+ T-cell responses in different conditions to the control condition. (c) Donut plots representing the relative magnitude (represented by the size) compared to control condition and polyfunctionality (Blue: 1 function; red: 2 functions; green: 3 functions; yellow: 4 functions) of HIV-specific CD8+ T cells from HIV controllers (n=11 individuals) and cART individuals (n=9 individuals, excluding 670115 with no Total HIV response) in control medium, in medium without glucose, and in the presence of menadione.

Figure 8

a) Fatty acid (BODIPY) uptake (MFI) by central memory CD8+ T cells from cART individuals (blue circles, n=7 individuals) after 48-72h incubation in the absence (control) or in presence of IL-15 [10ng/ml] (R&D). b) Oxygen consumption rates (two representative examples, means and standard deviation [n=3 replicates] at each time point are shown for each analysis, left), basal glycolysis and basal and maximal respiratory capacity (right, cells from n=8 individuals) by CD8+ T cells from cART-individuals pre-incubated or not with IL-15. Arrows indicate the time of addition of Oligomycin, FCCP and Rotenone/antimycin. c) TNFα production by HIV- and CMV-specific CD8+ T cells from cART (n=8 individuals) upon stimulation with pools of HIV-Gag (left) and CMVp665 peptides (right) in control medium. Cells had been pre-incubated (overnight) or not with IL-15. d) Representative example (left) and summary (cells from n=10 individuals) of viral suppression assays showing the capacity of CD8+ T cells from cART-individual ex vivo or pretreated with IL-15 to block HIV-1 infection of autologous CD4+ T cells. Data are means (and standard deviation for bar plots) of three replicates. (a-d) Each symbol represents values for cells from one individual. Medians are represented as horizontal lines. A non-parametric two-tailed Wilcoxon paired test was used to compare HIV-specific CD8+ T-cell responses in different conditions to the control condition.

Figure 1

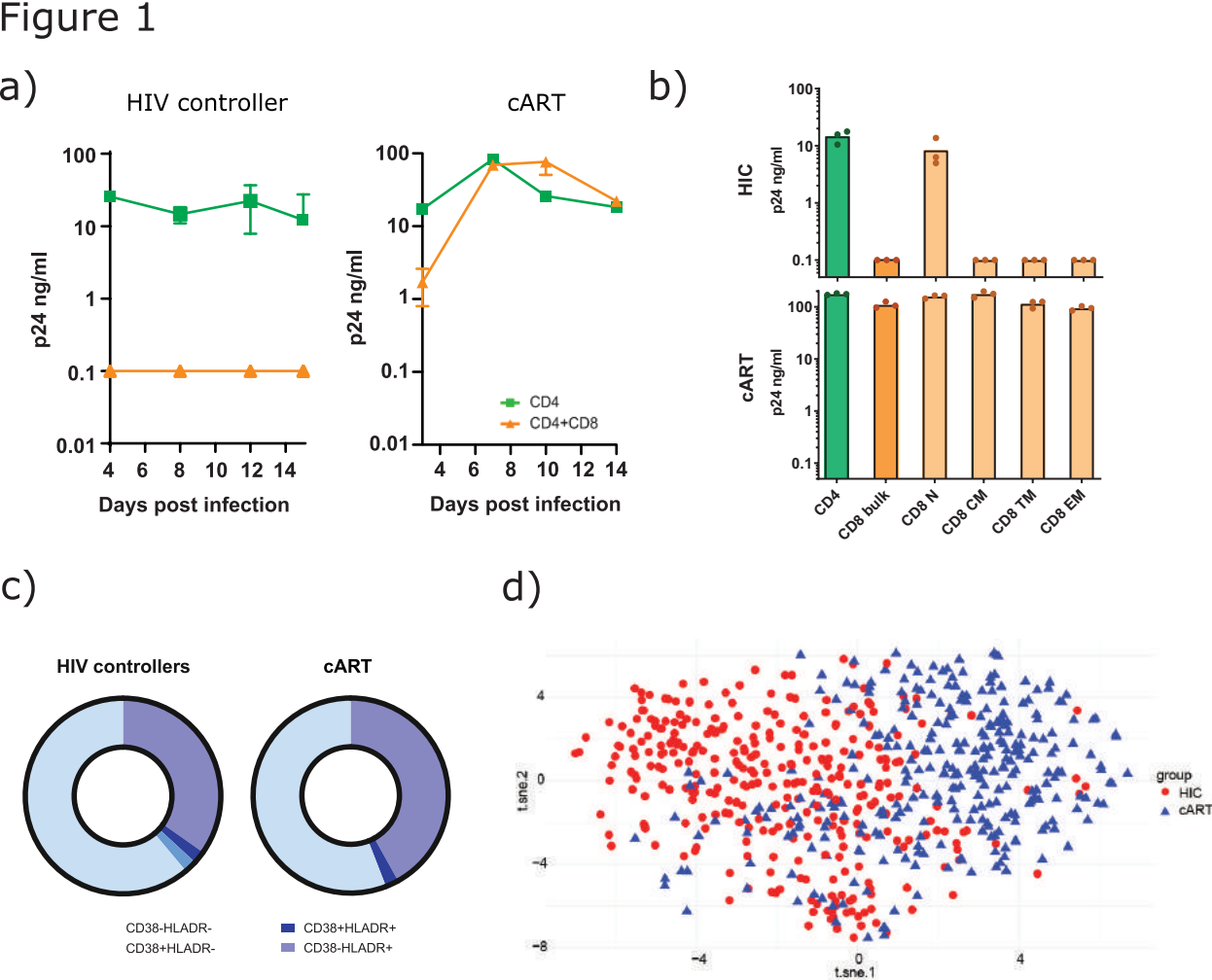

a)
HIV controller
cART
p24 ng/ml
Days post infection
CD4
CD4+CD8
b)
HIC
cART
p24 ng/ml
CD4
CD8 bulk
CD8 N
CD8 CM
CD8 TM
CD8 EM
c)
HIV controllers
cART
CD38-HLADR-
CD38+HLADR-
CD38+HLADR+
CD38-HLADR+
d)
t.sne.1
t.sne.2
group
HIC
cART

FIGURE 2

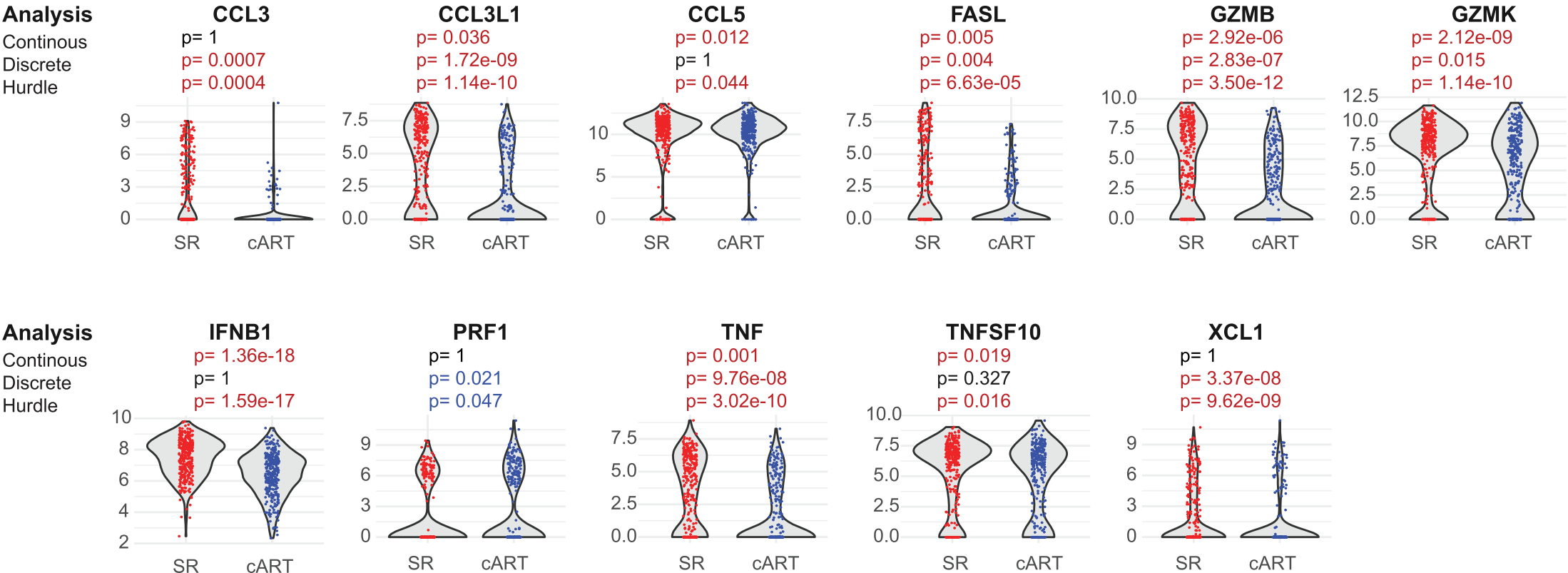

Analysis
Continous
Discrete
Hurdle
CCL3
p= 1
p= 0.0007
p= 0.0004
CCL3L1
p= 0.036
p= 1.72e-09
p= 1.14e-10
CCL5
p= 0.012
p= 1
p= 0.044
FASL
p= 0.005
p= 0.004
p= 6.63e-05
GZMB
p= 2.92e-06
p= 2.83e-07
p= 3.50e-12
GZMK
p= 2.12e-09
p= 0.015
p= 1.14e-10
IFNB1
p= 1.36e-18
p= 1
p= 1.59e-17
PRF1
p= 1
p= 0.021
p= 0.047
TNF
p= 0.001
p= 9.76e-08
p= 3.02e-10
TNFSF10
p= 0.019
p= 0.327
p= 0.016
XCL1
p= 1
p= 3.37e-08
p= 9.62e-09
SR
cART

FIGURE 3

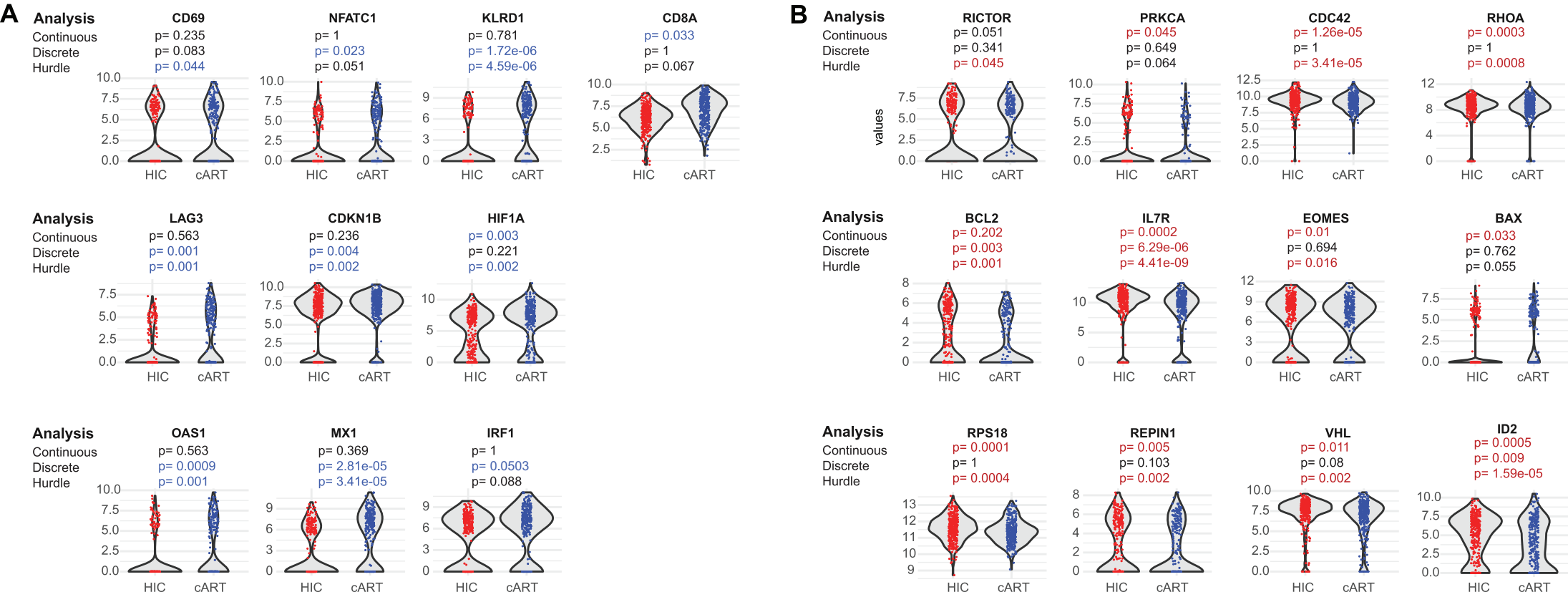

A
Analysis
Continuous
Discrete
Hurdle
CD69
p= 0.235
p= 0.083
p= 0.044
NFATC1
p= 1
p= 0.023
p= 0.051
KLRD1
p= 0.781
p= 1.72e-06
p= 4.59e-06
CD8A
p= 0.033
p= 1
p= 0.067
LAG3
p= 0.563
p= 0.001
p= 0.001
CDKN1B
p= 0.236
p= 0.004
p= 0.002
HIF1A
p= 0.003
p= 0.221
p= 0.002
OAS1
p= 0.563
p= 0.0009
p= 0.001
MX1
p= 0.369
p= 2.81e-05
p= 3.41e-05
IRF1
p= 1
p= 0.0503
p= 0.088
HIC
cART
B
Analysis
Continuous
Discrete
Hurdle
values
RICTOR
p= 0.051
p= 0.341
p= 0.045
PRKCA
p= 0.045
p= 0.649
p= 0.064
CDC42
p= 1.26e-05
p= 1
p= 3.41e-05
RHOA
p= 0.0003
p= 1
p= 0.0008
BCL2
p= 0.202
p= 0.003
p= 0.001
IL7R
p= 0.0002
p= 6.29e-06
p= 4.41e-09
EOMES
p= 0.01
p= 0.694
p= 0.016
BAX
p= 0.033
p= 0.762
p= 0.055
RPS18
p= 0.0001
p= 1
p= 0.0004
REPIN1
p= 0.005
p= 0.103
p= 0.002
VHL
p= 0.011
p= 0.08
p= 0.002
ID2
p= 0.0005
p= 0.009
p= 1.59e-05
HIC
cART

Figure 4

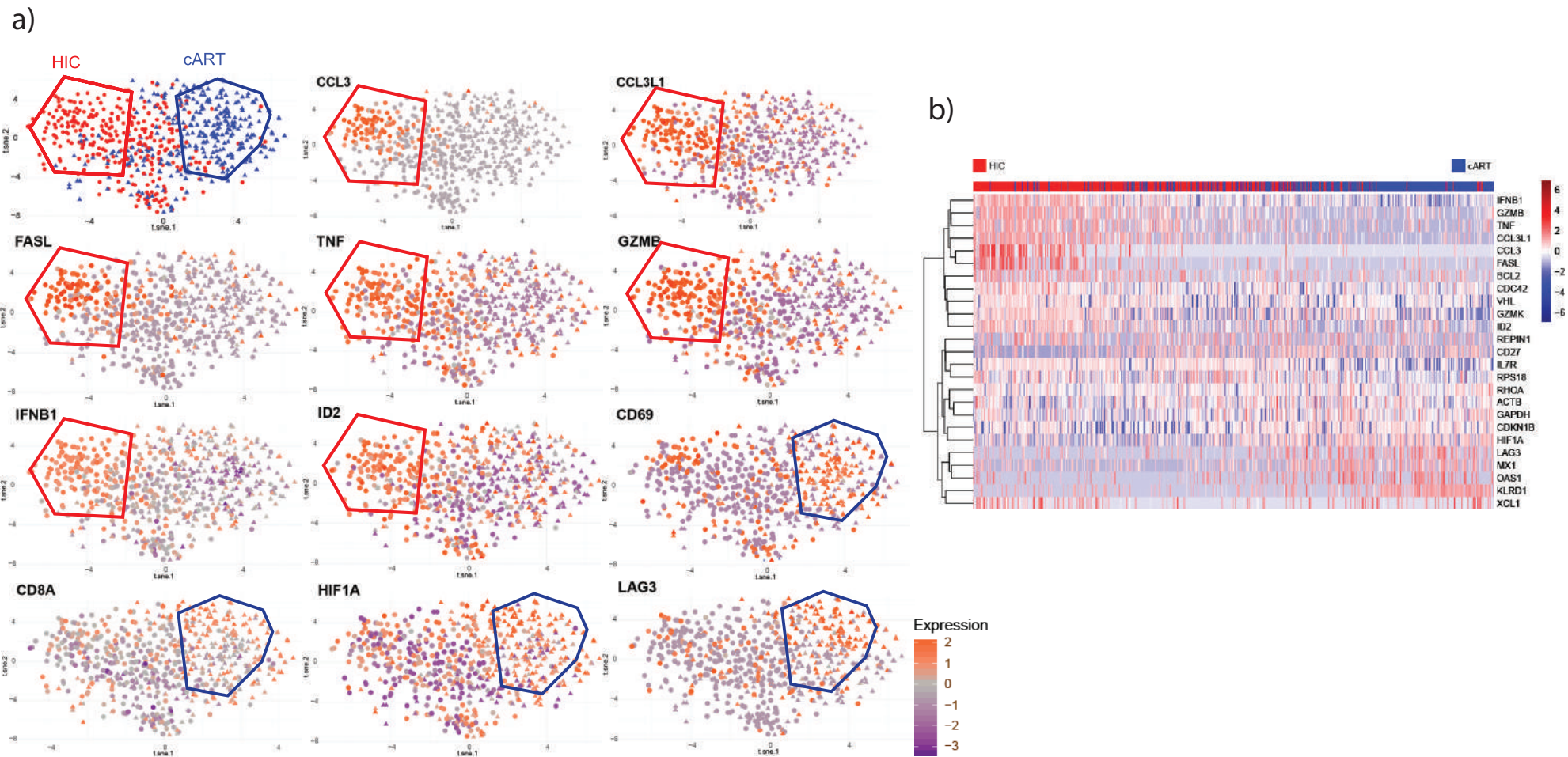

a)
HIC
cART
CCL3
CCL3L1
FASL
TNF
GZMB
IFNB1
ID2
CD69
CD8A
HIF1A
LAG3
t.sne.1
t.sne.2
b)
HIC
cART
IFNB1
GZMB
TNF
CCL3L1
CCL3
FASL
BCL2
CDC42
VHL
GZMK
ID2
REPIN1
CD27
IL7R
RPS18
RHOA
ACTB
GAPDH
CDKN1B
HIF1A
LAG3
MX1
OAS1
KLRD1
XCL1
Expression

FIGURE 5

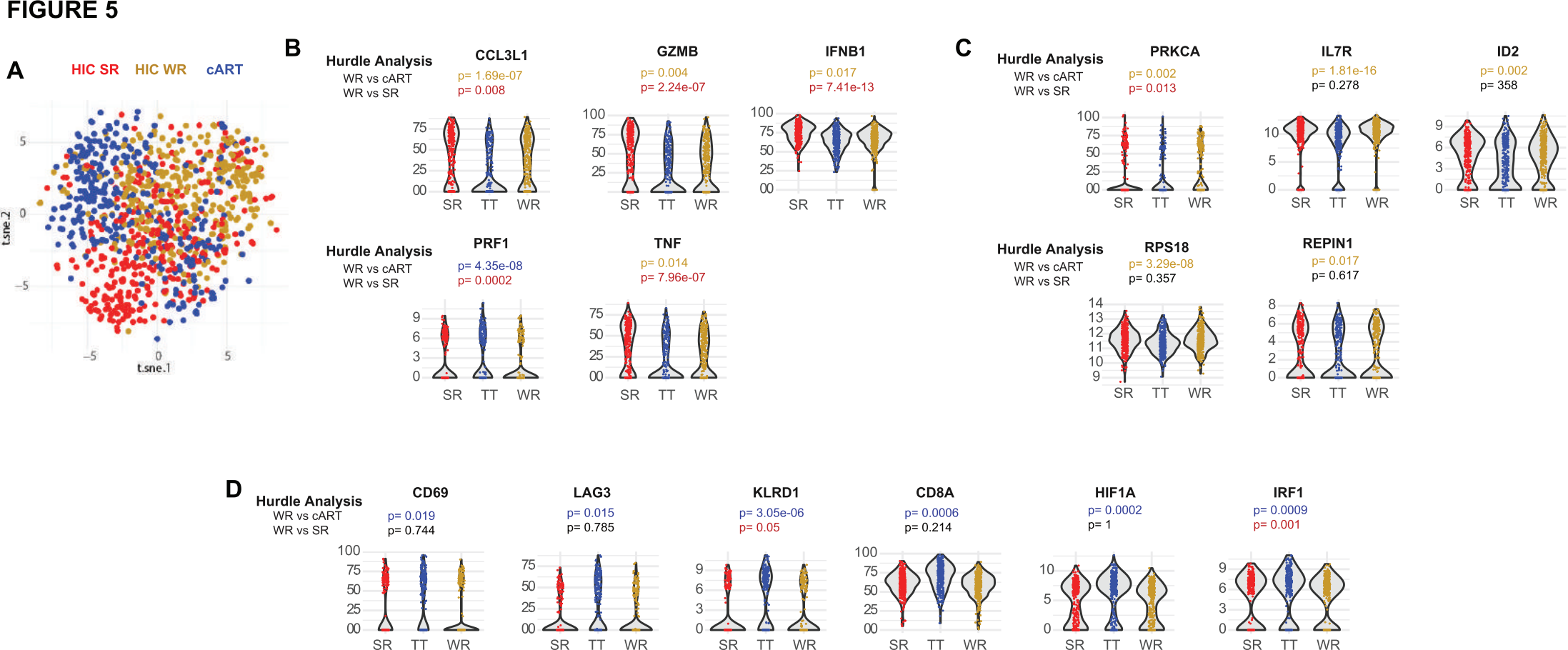

A
HIC SR
HIC WR
cART
t.sne.2
t.sne.1
B
Hurdle Analysis
WR vs cART
WR vs SR
CCL3L1
p= 1.69e-07
p= 0.008
GZMB
p= 0.004
p= 2.24e-07
IFNB1
p= 0.017
p= 7.41e-13
PRF1
p= 4.35e-08
p= 0.0002
TNF
p= 0.014
p= 7.96e-07
C
PRKCA
p= 0.002
p= 0.013
IL7R
p= 1.81e-16
p= 0.278
ID2
p= 0.002
p= 358
RPS18
p= 3.29e-08
p= 0.357
REPIN1
p= 0.017
p= 0.617
D
CD69
p= 0.019
p= 0.744
LAG3
p= 0.015
p= 0.785
KLRD1
p= 3.05e-06
p= 0.05
CD8A
p= 0.0006
p= 0.214
HIF1A
p= 0.0002
p= 1
IRF1
p= 0.0009
p= 0.001
SR
TT
WR

Figure 6

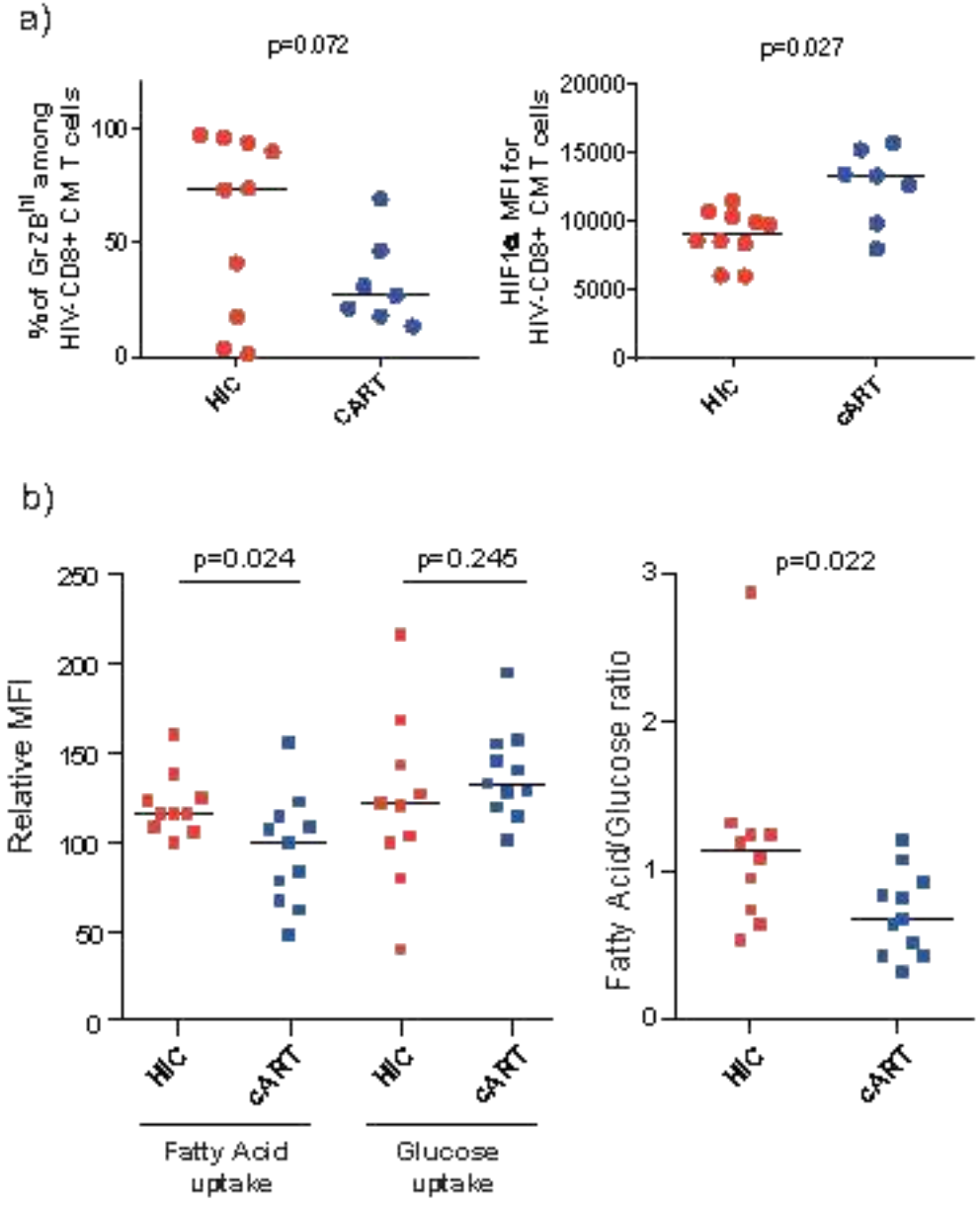

a)
p=0.072
% of GrZB^hi among HIV-CD8+ CM T cells
100
50
0
HIC
cART
p=0.027
HIF1α MFI for HIV-CD8+ CM T cells
20000
15000
10000
5000
0
HIC
cART
b)
p=0.024
p=0.245
Relative MFI
250
200
150
100
50
0
HIC
cART
HIC
cART
Fatty Acid uptake
Glucose uptake
p=0.022
Fatty Acid/Glucose ratio
3
2
1
0
HIC
cART

Figure 7

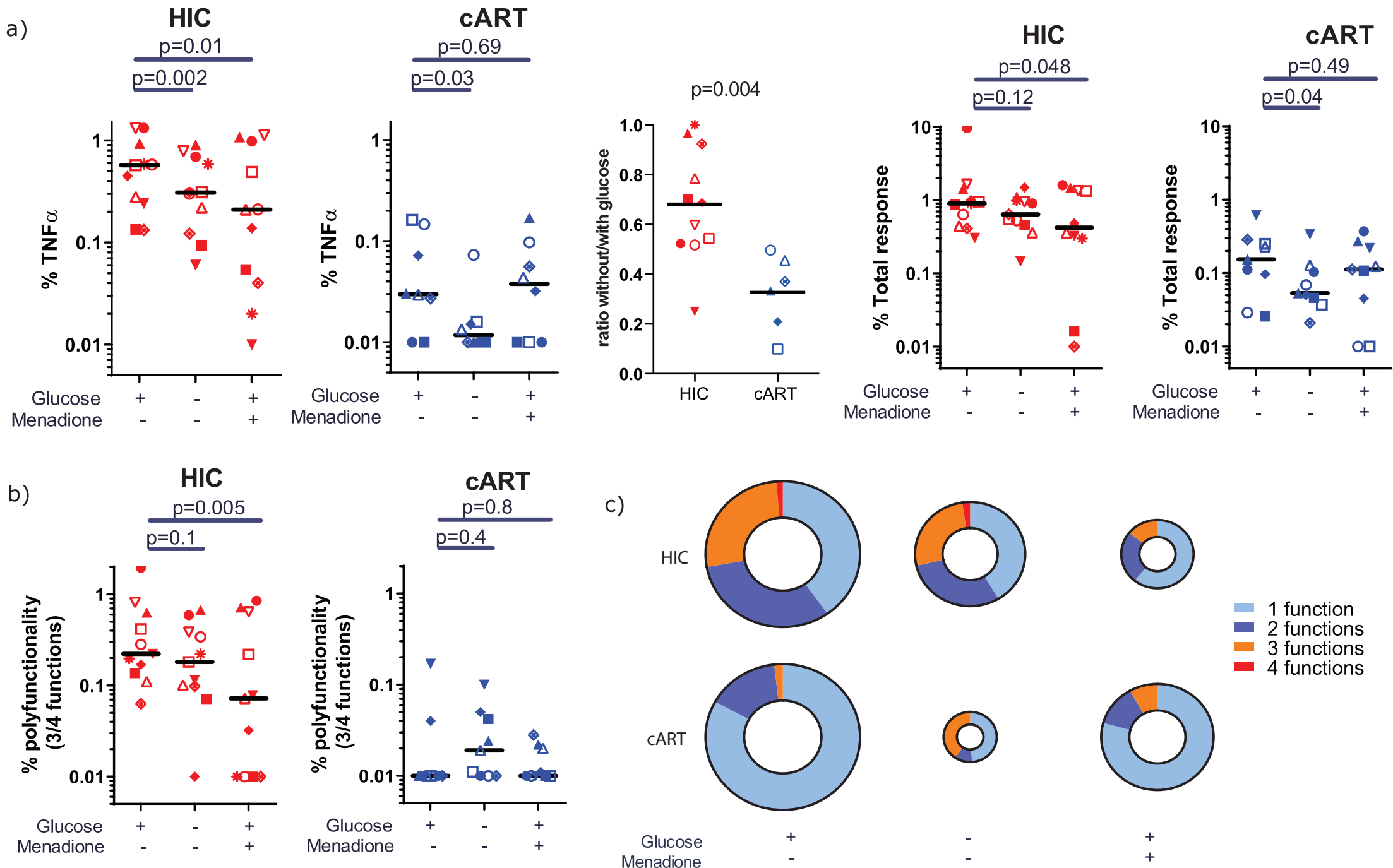
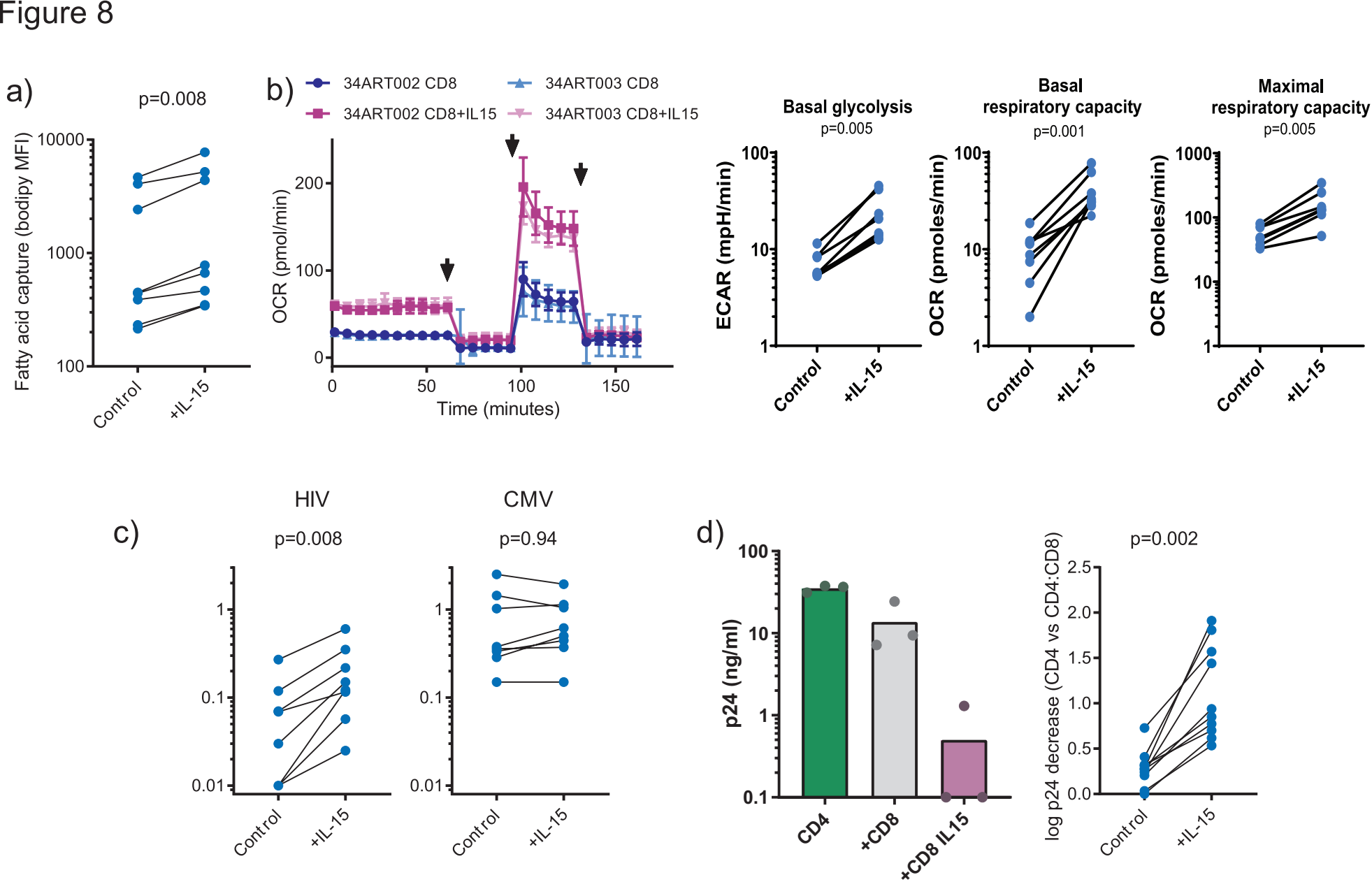

a)
HIC
p=0.01
p=0.002
cART
p=0.69
p=0.03
% TNFα
1
0.1
0.01
Glucose + - +
Menadione - - +
p=0.004
ratio without/with glucose
1.0
0.8
0.6
0.4
0.2
0.0
HIC
cART
HIC
p=0.048
p=0.12
cART
p=0.49
p=0.04
% Total response
10
1
0.1
0.01
b)
HIC
p=0.005
p=0.1
cART
p=0.8
p=0.4
% polyfunctionality (3/4 functions)
c)
HIC
cART
1 function
2 functions
3 functions
4 functions

Figure 8


a)
p=0.008
Fatty acid capture (bodipy MFI)
10000
1000
100
Control
+IL-15
b)
34ART002 CD8
34ART002 CD8+IL15
34ART003 CD8
34ART003 CD8+IL15
OCR (pmol/min)
200
100
0
0
50
100
150
Time (minutes)
Basal glycolysis
p=0.005
ECAR (mpH/min)
100
10
1
Control
+IL-15
Basal respiratory capacity
p=0.001
OCR (pmoles/min)
100
10
1
Control
+IL-15
Maximal respiratory capacity
p=0.005
OCR (pmoles/min)
1000
100
10
1
Control
+IL-15
c)
HIV
p=0.008
1
0.1
0.01
Control
+IL-15
CMV
p=0.94
1
0.1
0.01
Control
+IL-15
d)
p24 (ng/ml)
100
10
1
0.1
CD4
+CD8
+CD8 IL15
p=0.002
log p24 decrease (CD4 vs CD4:CD8)
2.5
2.0
1.5
1.0
0.5
0.0
Control
+IL-15